2018

A Sierpinski Mandelbrot spiral for rational maps of the form $Z^N + \lambda / Z^D$

BOSTON UNIVERSITY

GRADUATE SCHOOL OF ARTS AND SCIENCES

Dissertation

A SIERPINSKI MANDELBROT SPIRAL FOR RATIONAL MAPS OF THE FORM $Z^N + \lambda/Z^D$

by

ERIC CHANG

Bachelor of Science, Columbia University, 2004
Master of Arts, Western New England University, 2010

Submitted in partial fulfillment of the

requirements for the degree of

Doctor of Philosophy

2018

Approved by

First Reader

Robert L. Devaney, PhD
Professor of Mathematics

Second Reader

Paul Blanchard, PhD
Professor of Mathematics

Third Reader

G. Richard Hall, PhD
Professor of Mathematics

Acknowledgments

Over the past seven years I have received support and advice from too many people to name here, but I will make an attempt. Bob Devaney has been the best advisor a student could wish for. Without him, I would still be looking for a research topic, conferences to attend, and a job. Dick Hall, Gene Wayne, Margaret Beck, Paul Blanchard, and Tasso Kaper are my touchstones whenever I need to make a decision related to research, teaching, or living. I would get a WWBDGMPTD bracelet if my wrist were larger.

Becoming Bob's student was like joining a family. I would like to thank Núria Fagella and Xavier Jarque for running the excellent Topics in Complex Dynamics school and giving me unrealistic expectations for all future conferences. Visca Catalunya lliure!

The math faculty at Western New England University have a fever, and the only cure is - there is no cure. They love math and teaching math, and more importantly, it comes across with such sincerity that α in the corresponding SIR model would be dangerously high. Caleb Shor and Tom Hull, you guys rock.

Some people said that going back to school for a PhD in math after earning a BS in engineering seven years ago would be difficult. They were resoundingly correct. Osman Chaudhary, Tommy McCauley, and Siragan Gailus, I would not have made it to this point without you.

My mom is awesome. Thanks, mom.

A SIERPINSKI MANDELBROT SPIRAL FOR RATIONAL MAPS OF THE FORM $Z^N + \lambda/Z^D$

ERIC CHANG

Boston University, Graduate School of Arts and Sciences, 2018

Major Professor: Robert L. Devaney, PhD
Professor of Mathematics

ABSTRACT

We identify three structures that lie in the parameter plane of the rational map $F(z) = z^n + \lambda/z^d$, for which z is a complex number, λ a complex parameter, $n \geq 4$ is even, and $d \geq 3$ is odd.

There exists a Sierpindelbrot arc, an infinite sequence of pairs of Mandelbrot sets and Sierpinski holes, that limits to the parameter at the end of the arc.

There exists as well a qualitatively different Sierpindelbrot arc, an infinite sequence of pairs of Mandelbrot sets and Sierpinski holes, that limits to the parameter at the center of the arc.

Furthermore, there exist infinitely many arcs of each type. A parameter can travel along a continuous path from the Cantor set locus, along infinitely many arcs of the first type in a successively smaller region of the parameter plane, while passing through an arc of the second type, to the parameter at the center of the latter arc. This infinite sequence of Sierpindelbrot arcs is a Sierpinski Mandelbrot spiral.

Contents

List of Figures

List of Abbreviations

$\mathcal{A}$	.....	An annulus in the parameter plane
B_λ	.....	The immediate basin of attraction of ∞
c^λ	.....	A critical point that varies analytically with λ
$\mathcal{E}^1$	.....	The McMullen domain
$\mathcal{E}^k, k \geq 2$	.....	A Sierpinksi hole of escape time k
$\mathcal{J}(F_\lambda)$	.....	The Julia set of F_λ
L^λ	.....	The left wedge
$\mathcal{M}^k, k \geq 2$	.....	A Mandelbrot set of base period k
$\mathcal{O}$	.....	An annulus in the parameter plane
p^λ	.....	A prepole that varies analytically with λ
$\mathbb{R}$	.....	The real line
R_i^λ	.....	A right wedge
$\mathcal{S}_n$	.....	A sector in the parameter plane that varies with n
T_λ	.....	The trap door
$T_\mathcal{A}$	.....	An open disk subset of the trap door
v^λ	.....	A critical value that varies analytically with λ

Chapter 1

Introduction

1.1 Singularly Perturbed Rational Maps

It is known that there are several intriguing geometric structures surrounding the negative real axis in the parameter plane for rational maps of the form $F_\lambda(z) = z^n + \lambda/z^d$. In the case where n and d are even, it has been shown in (Devaney, 2004) that there is a "Cantor necklace" that lies along the negative real axis in the parameter plane and a principal Mandelbrot set along the positive axis. A Cantor necklace is a set that is a continous image of the Cantor middle-thirds set to which is adjoined countably many open disks in the plane in place of the removed open intervals along the real line. For parameters inside these open disks (which we call Sierpinski holes), the Julia set of F_λ is known to be a Sierpinski curve (i.e., is homeomorphic to the Sierpinski carpet fractal), and the different dynamical behaviors on these Julia sets is completely understood (Moreno Rocha, 2013). In the case where n is odd and d is even, there is no such Cantor necklace; rather there are now two principal Mandelbrot sets, one along the positive real axis and the other along the negative real axis. As a consequence, the dynamical behavior for these parameters is very different from the behavior when n and d are both even. Thus the remaining case is when n is even and d is odd; we look at a specific instance of this.

As when d is even, we again have a principal Mandelbrot set straddling the positive real axis. But the structure on and around the negative real axis is very different.

When $n \geq 2$ is even and $d \geq 3$ is odd, there exists a "Mandelpinski maze" (MS maze) in a neighborhood of the negative real axis in the parameter plane. (Devaney, 2016) proves the existence of a "Sierpindelbrot arc" (SM arc), which is the building block of a MS maze.

This paper shows that, by restricting n to be at least 4, one can expand on the construction and find infinitely many SM arcs in the parameter plane. Each SM arc is an infinite sequence of pairs of Sierpinski holes and Mandelbrot sets of increasingly higher escape time or base period. By considering the λ at the center of each Sierpinski hole, there exists a corresponding sequence of λ values. Each SM arc, as a sequence of parameter values λ, tends to a limit λ such that, in dynamical space, some iterate of the critical value is a fixed point.

Furthermore, the expanded construction allows for the proof of the existence of a second type of SM arc different from the first. This leads to the existence of a spiral of infinitely many SM arcs of the first type that pass through a single SM arc of the second type. The spiral is an infinite sequence of SM arcs (i.e. a sequence of sequences) with limit λ corresponding to increasingly more iterations before the critical value lands on a fixed point. The spiral, as a sequence of SM arcs, tends to a limit SM arc that itself tends to a λ such that, in dynamical space, the critical value *is* a fixed point. In the parameter plane, each SM arc in the sequence exists in a successively smaller region as the SM arcs tend to the aforementioned limit λ in a spiraling pattern, thus the name "Sierpinski Mandelbrot spiral" (SM spiral).

We first prove the existence of a spiral for the case $n = 4$ and $d = 3$. We then find analogues of the arguments to prove the existence of a spiral for the general case $n \geq 4$ is even and $d \geq 3$ is odd, with a specific set of exceptions for which the analogues do not hold. We finally adjust the argument to find exceptional spirals for almost every exception.

1.2 The Escape Trichotomy

We consider

$$F_\lambda(z) = z^n + \frac{\lambda}{z^d}$$

where $z \in \mathbb{C}$, $\lambda \in \mathbb{C}$ is nonzero, $n \geq 4$ is even and $d \geq 3$ is odd.

When $|z|$ is large, we have that $|F_\lambda(z)| > |z|$, so the point at ∞ is an attracting fixed point in the Riemann sphere. We denote the immediate basin of attraction of ∞ by B_λ. There is also a pole at the origin for this map, and so there is a neighborhood of the origin that is mapped into B_λ. If the preimage of B_λ surrounding the origin is disjoint from B_λ, we call this region the trap door and denote it by T_λ.

The Julia set of $F_\lambda, J(F_\lambda)$, has several equivalent definitions. $J(F_\lambda)$ is the set of all points at which the family of iterates of F_λ fails to be a normal family in the sense of Montel. Equivalently, $J(F_\lambda)$ is the closure of the set of repelling periodic points of F_λ, and it is also the boundary of the set of all points whose orbits tend to ∞ under iteration of F_λ, not just those in the boundary of B_λ. See (Milnor, 2006).

One checks that there are $n + d$ critical points that are given by

$$c^\lambda = \left(\frac{d\lambda}{n}\right)^{\frac{1}{n+d}}$$

with the corresponding critical values given by

$$v^\lambda = \frac{(d+n)\lambda^{\frac{n}{n+d}}}{d^{\frac{d}{n+d}} n^{\frac{n}{n+d}}}.$$

There are also $n + d$ prepoles given by

$$p^\lambda = (-\lambda)^{\frac{1}{n+d}}.$$

We denote the critical point that lies in $\mathbb{R}^-$ when $\lambda \in \mathbb{R}^-$ by c_0^λ. The other critical points are denoted by by c_j^λ where $-\frac{n+d-1}{2} \leq j \leq \frac{n+d-1}{2}$ and the c_j are arranged in clockwise order as j increases. We denote by v_j^λ the critical value that is the image of c_j^λ.

We denote the prepole that lies in $\mathbb{R}^+$ when $\lambda \in \mathbb{R}^-$ by $p_{\frac{n+d-1}{2}}^\lambda$. The other prepoles are denoted by p_j^λ where again $-\frac{n+d-1}{2} \leq j \leq \frac{n+d-1}{2}$ and the p_j are arranged in clockwise order as j increases.

The straight ray extending from the origin to ∞ and passing through a critical point c^λ is called a critical point ray. These rays are mapped two-to-one onto the portion of the straight ray from the origin to ∞ that starts at the critical value $F_\lambda(c^\lambda)$ and extends to ∞ beyond this critical value. A similar straight line extending from 0 to ∞ and passing through a prepole p^λ is a prepole ray, and these rays are mapped one-to-one onto the entire straight line passing through both the origin and the point $(-\lambda)^{\frac{n}{n+d}}$.

Let ω be an $(n+d)^{th}$ root of unity. Then we have $F_\lambda(\omega z) = \omega^n F_\lambda(z)$, and so it follows that the dynamical plane is symmetric under the rotation $z \mapsto \omega z$. In particular, all of the critical orbits have similar fates. If one critical orbit tends to ∞, then all must do so. If one critical orbit tends to an attracting cycle of some period, then all other critical orbits also tend to an attracting cycle, though these other cycles may have different periods. Nonetheless, the points on these attracting cycles are all symmetrically located with respect to the rotation by ω. As a consequence, each of B_λ, T_λ, and $J(F_\lambda)$ are symmetric under rotation by ω. Similarly, one checks easily that the parameter plane is symmetric under the rotation $\lambda \mapsto \nu\lambda$ where ν is an $(n-1)^{th}$ root of unity. The parameter plane is also symmetric under complex conjugation $\lambda \mapsto \overline{\lambda}$.

The Escape Trichotomy (Devaney et al., 2005) holds for this rational map. The

first scenario in this trichotomy occurs when one and hence, by symmetry, all of the critical values lie in B_λ. In this case it is known that $J(F_\lambda)$ is a Cantor set. The corresponding set of λ in the parameter plane is denoted by $\mathcal{C}$ and called the Cantor set locus. The second scenario is that the critical values all lie in T_λ (which we assume is disjoint from B_λ). In this case the Julia set is a Cantor set of simple closed curves surrounding the origin. This can only happen when $n, d \geq 2$ but not both equal to 2 (McMullen, 1988). We call the region $\mathcal{E}^1$ in the parameter plane where this occurs the "McMullen domain"; it is known that $\mathcal{E}^1$ is an open disk surrounding the origin (Devaney, 2005). The third scenario is that the orbit of a critical point enters T_λ at iteration 2 or higher. Then, by the above symmetry, all such critical orbits do the same. In this case, it is known that the Julia set is a Sierpinski curve (Devaney and Look, 2006), i.e., a set that is homeomorphic to the well known Sierpinski carpet fractal. The regions in the parameter plane for which this happens are the open disks that we call Sierpinski holes (Roesch, 2006). If the critical orbits do not escape to ∞, then it is known (Devaney and Russell, 2013) that the Julia set is a connected set. Thus we call the set of parameters for which the critical orbits either do not escape or else enter the trap door at iteration 2 or higher the connectedness locus. This is the complement of $\mathcal{C} \cup \mathcal{E}^1$.

In (Devaney, 2006) it has been shown that there are $n-1$ principal Mandelbrot sets in the parameter plane for these maps. These are symmetrically located by the rotation νz around the origin and extend from the Cantor set locus down to the McMullen domain.

For more details about the dynamical properties of these maps and the structure of the parameter plane, see (Devaney, 2013).

Chapter 2

The Case $n = 4$ and $d = 3$

2.1 Overview

As in (Devaney, 2016), we construct sets in dynamical space, the union of which is called the "bowtie." We then prove that certain properties about the bowtie hold in a sector of an annulus in the parameter plane. Those properties are used to construct a dynamical arc that proves the existence of a corresponding parameter arc of Sierpinski holes and Mandelbrot sets in that subset of the parameter plane.

Beyond (Devaney, 2016), we see that the bowtie can be used to construct a qualitatively different dynamical arc that proves the existence of corresponding qualitatively different parameter arc. Furthermore, there are infinitely many copies of each arc, and some of those infinitely many arcs spiral toward a fixed point in the dynamical space.

In particular, we construct the $\overline{0}$ TL arc in the dynamical plane and use it to prove the existence of the $\overline{0}$ SM arc in the parameter plane. We then construct the $\overline{1}$ TL arc, and show that the two types of arcs together comprise the $\overline{1}$ TL spiral. Next, we find the spiral's preimage, the $0\overline{1}$ TL spiral, and use it to prove the existence of the $0\overline{1}$ SM spiral in the parameter plane. Finally, we use symmetry to establish the existence of infinitely many spirals.

We narrow our focus to the specific case

$$F_\lambda(z) = z^4 + \frac{\lambda}{z^3}$$

where $z \in \mathbb{C}$, $\lambda \in \mathbb{C}$ is nonzero.

There are three symmetrically located Mandelbrot sets in the parameter plane. Figure 2·1 depicts the Mandelbrot sets and the rest of the connectedness locus, the McMullen domain, the Cantor set locus. Because of the $\lambda \mapsto \nu\lambda$ symmetry in the parameter plane, we need only be concerned with $\frac{2\pi}{3} \leq \text{Arg } \lambda \leq \frac{4\pi}{3}$.

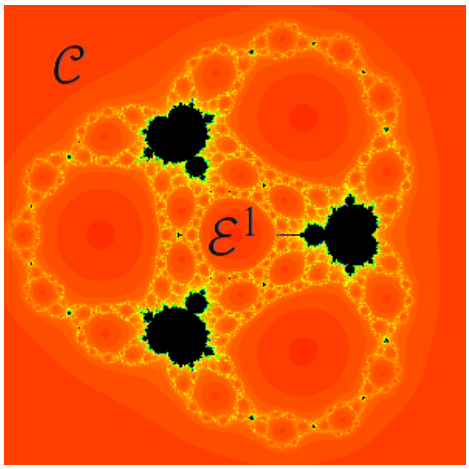

Figure 2·1: Parameter plane for $z^4 + \lambda/z^3$

One checks that there are seven critical points with corresponding critical values and seven prepoles, denoted as in section 1.2. In particular, c_0^λ lies on $\mathbb{R}^-$ when $\lambda \in \mathbb{R}^-$ and varies analytically with λ.

The critical values of F_λ are given by $v^\lambda = \kappa\lambda^{4/7}$ where κ is the constant $\frac{7}{4^{4/7}3^{3/7}}$. One computes that $\kappa \approx 1.98$. When $\lambda \in \mathbb{R}^-$, the critical point c_0^λ lies between the two prepole rays passing through p_0^λ and p_{-1}^λ.

2.2 Phase One: The Bowtie Construction

Let $\mathcal{O}$ be the annulus in the parameter plane given by $10^{-10} \leq |\lambda| \leq 2$. Also, let $\mathcal{A}$ be the annulus in the dynamical plane given by $\kappa 10^{-4} \leq |z| \leq \kappa 4^{4/7}$.

Proposition 2.2.1.
1. For any $\lambda \in \mathcal{O}$, all points on the outer circular boundary of $\mathcal{A}$ lie in B_λ, while all points on the inner circular boundary of $\mathcal{A}$ lie in T_λ. Moreover, F_λ maps each of these boundaries strictly outside the boundary of $\mathcal{A}$.
2. If λ lies on the inner circular boundary of $\mathcal{O}$, then v^λ lies on the inner circular boundary of $\mathcal{A}$ and so λ lies in the McMullen domain.
3. If λ lies on the outer circular boundary of $\mathcal{O}$, then v^λ lies on the outer circular boundary of $\mathcal{A}$ and so λ lies in the Cantor set locus in the parameter plane.

Proof. First, if $|z| = \tau\kappa 4^{4/7}$ for any $\tau \geq 1$, we have for each $\lambda \in \mathcal{O}$:

$$\begin{aligned} |F_\lambda(z)| &\geq |\tau^4\kappa^4 4^{16/7}| - \frac{\lambda}{\tau^3\kappa^3 4^{12/7}} \\ &\geq \tau^4 1.9^4 4^{16/7} - \left|\frac{2}{\tau^3\kappa^3 4^{12/7}}\right| \\ &\geq 300\tau^4 - \frac{1}{35\tau^3} \\ &> 299\tau \\ &> \tau\kappa 4^{4/7} = |z| \end{aligned}$$

So all points outside the circle $|z| = \kappa 4^{4/7}$ lie in B_λ when $\lambda \in \mathcal{O}$.

Similarly, if $|z| = \kappa 10^{-4}$, then we have

$$|F_\lambda(z)| \geq \frac{|\lambda|}{\kappa^3 10^{-12}} - \kappa^4 10^{-16} \geq \frac{10^{-10}}{\kappa^3 10^{-12}} - \kappa^4 10^{-16} \geq 100/\kappa^2 - \epsilon$$

where $\epsilon \approx 16(10^{-16})$. So this inner boundary is mapped into B_λ, and so are all smaller circles around the origin. Hence this circle lies in T_λ (when λ lies in the connectedness locus).

Now if λ lies on the inner circular boundary of $\mathcal{O}$, then $|\lambda| = 10^{-10}$ so that $|v^\lambda| = \kappa 10^{-40/7}$. Hence, for these λ-values, $v^\lambda \in T_\lambda$ and λ therefore lies in the McMullen domain. If λ lies on the outer circular boundary of $\mathcal{O}$, then $|\lambda| = 2$ so

that $|v^\lambda| = \kappa 4^{4/7}$ and thus this boundary circle lies in the Cantor set locus in the parameter plane. $\square$

Due to the threefold symmetry resulting from $n = 4$, we need only look at λ in $\mathcal{S}_4$ given by $\frac{2\pi}{3} \leq \text{Arg } \lambda \leq \frac{4\pi}{3}$. Altogether, we restrict attention to the region $\mathcal{S}_4 \bigcap \mathcal{O}$.

We now describe the bowtie: four sets in the dynamical plane consisting of the left wedge, right wedge, upper right wedge, and knot. For any parameter in $\mathcal{S}_4 \bigcap \mathcal{O}$:

Let the left wedge, L^λ, be the closed portion of the wedge in the annulus $\mathcal{A}$ in dynamical space that is bounded by the two prepole rays through p_0 and p_{-1}. When $\lambda \in \mathbb{R}^-$, L^λ is thus bounded by the rays extending from 0 and passing through $\exp(2\pi i(6/14))$ and $\exp(2\pi i(8/14))$. So the critical point c_0 lies in the interior of L^λ.

Next, let the right wedge, R_0^λ, be the closed portion of the wedge in $\mathcal{A}$ that is bounded by the critical point rays passing through c_3 and c_{-3}. When $\lambda \in \mathbb{R}^-$, this wedge is bounded by the critical point rays extending from 0 and passing through $\exp(\pm(2\pi i(1/14))$. It is also bounded by the inner and outer portions of $\partial\mathcal{A}$ between $\exp(\pm(2\pi i(1/14))$. Note that R_0^λ is the symmetric image of L^λ under $z \mapsto -z$.

Let the upper right wedge, R_1^λ, be the closed portion of the wedge in $\mathcal{A}$ that is bounded by the critical point rays passing through c_2 and c_3. When $\lambda \in \mathbb{R}^-$, this wedge is bounded by the critical point rays extending from 0 and passing through $\exp(2\pi i(1/14))$ and $\exp(2\pi i(3/14))$.

Let the knot, $T_\mathcal{A}$, be the open portion of the trap door bounded by the annulus, $|z| < \kappa 10^{-4}$. Note that the inner boundary circle of the annulus lies inside T_λ.

Figure 2·2 conveys why $L^\lambda \cup T_\mathcal{A} \cup R_0^\lambda \cup R_1^\lambda$ is called the bowtie. Figure 2·2a shows the prepole and critical point rays. Note that the boundaries of $\mathcal{J}(F)$ are distinct from the annulus which makes up the inner and outer boundaries of the wedges, as seen in figure 2·2b.

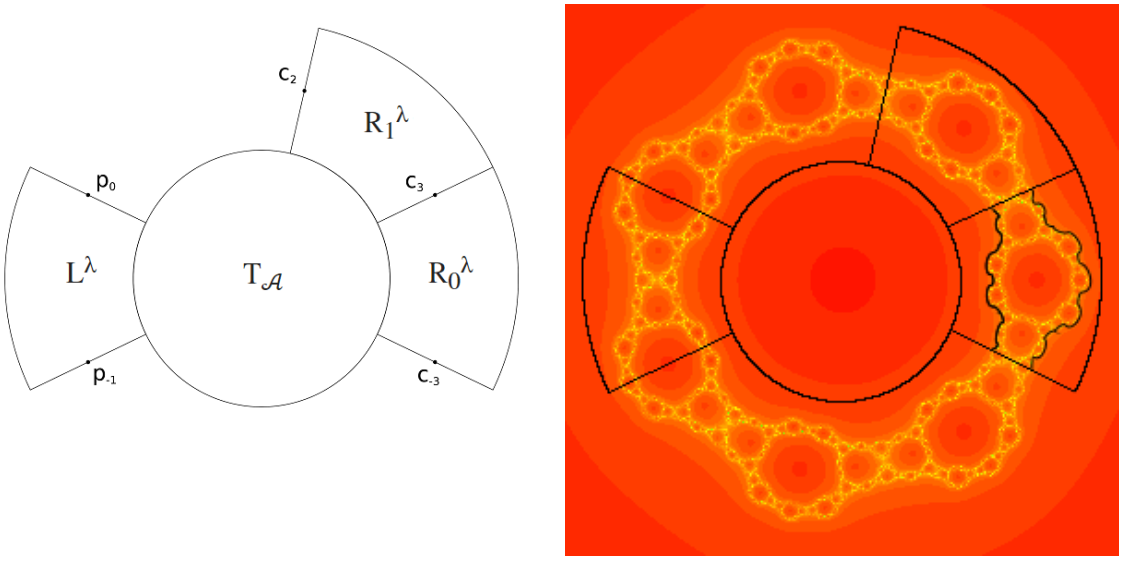

(a) A stylized depiction of the wedge construction

(b) The stylized construction in dynamical space

Figure 2·2: The bowtie construction

Proposition 2.2.2. *For each* $\lambda \in \mathcal{S}_4 \bigcap \mathcal{O}$

1. F_λ *maps* R_0^λ *in one-to-one fashion onto a region that contains the interior of* $R_0^\lambda \cup R_1^\lambda \cup L^\lambda \cup T_\mathcal{A}$*;*

2. F_λ *maps* R_1^λ *in one-to-one fashion onto a region that contains the interior of* $R_0^\lambda \cup R_1^\lambda \cup L^\lambda \cup T_\mathcal{A}$*;*

3. F_λ *maps* L^λ *two-to-one over a region that contains the interior of* R_0^λ*;*

4. As λ *winds once around the boundary of* $\mathcal{S}_4 \bigcap \mathcal{O}$*, the critical value* $F_\lambda(c_0^\lambda)$ *winds once around the boundary of* R_0^λ*, (i.e., the winding index of the vector connecting this critical value to the prepole* p_3^λ *lying in the interior of* R_0^λ *is one).*

Proof. For the first case, note that the straightline boundaries of R_0^λ are mapped two-to-one onto the critical point rays passing through v_3^λ and v_{-3}^λ. When $2\pi/3 < \text{Arg } \lambda \leq 4\pi/3$, these rays are disjoint from all of L^λ, R_0^λ, R_1^λ, and $T_\mathcal{A}$. When λ rotates clockwise to Arg $\lambda = 2\pi/3$, the sectors L^λ, R_0^λ, R_1^λ, and $T_\mathcal{A}$ rotate clockwise $2\pi(1/42)$ radians. The critical value ray v_3^λ rotates clockwise $2\pi(4/42)$ radians, and lies on the c_2^λ critical ray upper boundary of R_1^λ at $\exp(2\pi i(8/42))$. When λ rotates counter-clockwise to Arg $\lambda = 4\pi/3$, the sectors L^λ, R_0^λ, R_1^λ, and $T_\mathcal{A}$ rotate counter-clockwise $2\pi(1/42)$

radians. The critical value ray v_{-3}^{λ} rotates counter-clockwise $2\pi(4/42)$ radians, and still lies below the c_{-3}^{λ} critical ray boundary of R_0^{λ}. By the previous Proposition, the outer boundary curve of R_0^{λ} is mapped to an arc that lies in B_{λ} and also lies outside the circular boundaries of L^{λ}, R_0^{λ}, R_1^{λ}, and $T_{\mathcal{A}}$. This image arc connects the two critical value rays in B_{λ}, and lies to the right of these rays in B_{λ}. The inner boundary is mapped to a similar arc connecting these rays but now lying to the left. Consequently, the image of R_0^{λ} properly contains the interiors of L^{λ}, R_0^{λ}, R_1^{λ}, and $T_{\mathcal{A}}$.

For the second case, note that the straightline boundaries of R_1^{λ} are mapped two-to-one onto the critical point rays passing through v_3^{λ} and v_2^{λ}. When $2\pi/3 < \text{Arg } \lambda < 4\pi/3$, these rays are disjoint from all of L^{λ}, R_0^{λ}, R_1^{λ}, and $T_{\mathcal{A}}$. As above, when λ rotates clockwise to Arg $\lambda = 2\pi/3$, the sectors L^{λ}, R_0^{λ}, R_1^{λ}, and $T_{\mathcal{A}}$ rotate clockwise $2\pi(1/42)$ radians. The critical value ray v_3^{λ} has already been covered in the first case, as the lower boundary of R_1^{λ} and the upper boundary of R_0^{λ} are the same. When λ rotates counter-clockwise to Arg $\lambda = 4\pi/3$, the sectors L^{λ}, R_0^{λ}, R_1^{λ}, and $T_{\mathcal{A}}$ rotate counter-clockwise $2\pi(1/42)$ radians. The critical value ray v_2^{λ} rotates counter-clockwise $2\pi(4/42)$ radians, and lies on the c_{-3}^{λ} critical ray lower boundary of R_1^{λ} at $\exp(2\pi i(-2/42))$. By the previous Proposition, the outer boundary curve of R_1^{λ} is mapped to an arc that lies in B_{λ} and also lies outside the circular boundaries of L^{λ}, R_0^{λ}, R_1^{λ}, and $T_{\mathcal{A}}$. This image arc connects the two critical value rays in B_{λ}, and lies to the left of these rays in B_{λ}. The inner boundary is mapped to a similar arc connecting these rays but now lying to the right. Consequently, the image of R_1^{λ} properly contains the interiors of L^{λ}, R_0^{λ}, R_1^{λ}, and $T_{\mathcal{A}}$.

For the third case, we have that the straightline boundaries of L^{λ} contain the prepoles p_0^{λ} and p_{-1}^{λ}, which are both mapped to straight lines passing through the origin. In the case of p_0^{λ}, this straight line passes through $\exp(2\pi i(4/14))$ when $\lambda \in \mathbb{R}^-$. Then as Arg λ increases or decreases by at most $\pi/3$, the argument of this image line rotates by at most one-seventh of $\pi/3$ in the corresponding direction. Hence this line lies strictly outside R_0^{λ}. Note that the argument cannot be applied to R_1^{λ}, as the p_1^{λ} prepole ray and the c_2^{λ} critical point ray (the upper boundary of R_1^{λ}) both intersect $\exp(2\pi i(3/14))$ at $\lambda \in \mathbb{R}^-$. Similar arguments to the p_0^{λ} prepole ray work for the image of the p_{-1}^{λ} prepole ray. For the circular boundaries of L^{λ}, by the previous Proposition, they are both mapped to curves in B_{λ} that lie outside the outer boundary of $\mathcal{A}$, but now these curves are arcs that connect the image of the prepole rays passing to the right of these lines. Hence the image of L^{λ} covers R_0^{λ} two-to-one.

For the fourth case, when Arg $\lambda = 2\pi/3$, the image of c_0^{λ} lies on the ray passing

through $\exp(2\pi i(-4/42))$, and when Arg $\lambda = 4\pi/3$, the critical value lies on the complex conjugate ray. So, for these parameters, the critical value lies on the line that includes the straight line boundary of R_0^λ. For the circular boundaries of $\mathcal{S}_4 \bigcap \mathcal{O}$, the previous Proposition shows that the critical value now rotates around the corresponding circular boundary of R_0^λ. So the critical value does indeed wind once around R_0^λ.

□

2.3 Phase Two: The $\overline{0}$ Arc

Part one of Proposition 2.2.2 states that R_0^λ contains a preimage of itself, and so there must be a fixed point in R_0^λ. One checks easily that this fixed point is on the Julia set accessible from B_λ. We can now prove the existence of an arc of infinitely many preimages of L^λ and $T_\mathcal{A}$, with the initial pair of L^λ and $T_\mathcal{A}$ located near T_λ, and successive preimages extending to that fixed point. Inside R_0^λ there is a preimage of the region that contains the interior of $L^\lambda \cup T_\mathcal{A} \cup R_0^\lambda$. The prepole p_3^λ is inside the preimage of $T_\mathcal{A}$, so that we have the preimages of $L^\lambda \cup T_\mathcal{A} \cup R_0^\lambda$ in order of increasing $|z|$, i.e. $L^\lambda, T_\mathcal{A}$, then R_0^λ, which compactly contains the preimages of L^λ, $T_\mathcal{A}$, and R_0^λ (see figure 2·3b). Increasing $|z|$ is correct when λ lies on the real axis in the parameter plane, but not necessarily so for λ with imaginary component. It is more precise to say that the preimages are arranged in order along the arc extending from T_λ to B_λ.

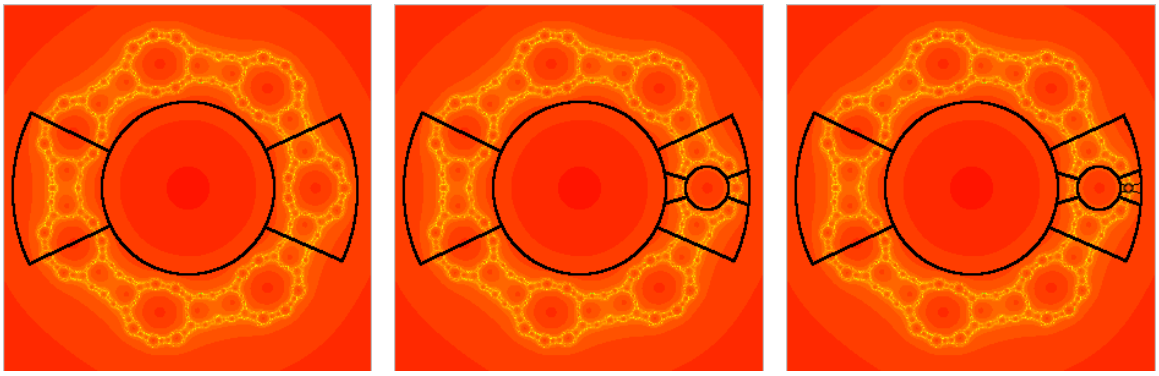

(a) The construction $L^\lambda, T_\mathcal{A}$, and R_0^λ

(b) $0L^\lambda, 0T_\mathcal{A}$, and $0R_0^\lambda$ inside R_0^λ

(c) $0_2L^\lambda, 0_2T_\mathcal{A}$, and $0_2R_0^\lambda$ inside $0R_0^\lambda$

Figure 2·3: Preimages of the right wedge

Continuing, inside the preimage of R_0^λ there is another preimage of the region that contains the interior of $L^\lambda \cup T_\mathcal{A} \cup R_0^\lambda$ in order along the arc. Inside the preimage of the preimage of R_0^λ there is another preimage of the region that contains the interior of $L^\lambda \cup T_\mathcal{A} \cup R_0^\lambda$ in order along the arc. And so on ...

It is useful to to refer to the preimages by their itineraries. In other words, inside R_0^λ is $0L^\lambda$, $0T_\mathcal{A}$, and $0R_0^\lambda$. A point in $0L^\lambda$ is in R_0^λ, and after one iteration is in L^λ. Similarly, a point in $0T_\mathcal{A}$ is in R_0^λ, and after one iteration is in $T_\mathcal{A}$. And a point in $0R_0^\lambda$ is in R_0^λ, and after one iteration is still in R_0^λ. Inside $0R_0^\lambda$ is $00L^\lambda, 00T_\mathcal{A}$, and $00R_0^\lambda$. A point inside these preimages is in R_0^λ, then R_0^λ, then L^λ, $T_\mathcal{A}$, or still R_0^λ respectively. We will use the notation 0_k to represent a sequence of k 0's (i.e., $00L^\lambda = 0_2L^\lambda$). Continuing, inside $00R_0^\lambda$, or $0_2R_0^\lambda$, is $0_3L^\lambda, 0_3T_\mathcal{A}$, and $0_3R_0^\lambda$.

This process continues iteratively as successive preimages of the region that contains the interior of $L^\lambda, T_\mathcal{A}$, and R_0^λ accumulate at the fixed point inside R_0^λ. As this arc consists of preimages named with only 0's that accumulate at the fixed point corresponding to the set with itinerary $000\ldots$, it is called the "$\overline{0}$ TL arc." This arc in dynamical space consists of $T_\mathcal{A}$ as well as infinitely many alternating preimages of

L^λ and $T_\mathcal{A}$ and bounded by B_λ on the right:

$$T_\mathcal{A} < 0L^\lambda < 0T_\mathcal{A} < 0_2L^\lambda < 0_2T_\mathcal{A} < 0_3L^\lambda < 0_3T_\mathcal{A} < \cdots < \text{f.p. in } R_0^\lambda < B_\lambda$$

Each TL arc is an infinite sequence of pairs of preimages of $T_\mathcal{A}$ and L^λ of increasingly higher iterations before z lands in L^λ or $T_\mathcal{A}$. By considering the z at the center of each preimage of $T_\mathcal{A}$, there exists a corresponding sequence of z values. Each TL arc, as a sequence of z, tends to the fixed point in R_0^λ or to one of its preimages.

The $\overline{0}\,TL$ arc in dynamical space quickly becomes hard to see due to the difference in scale of each successive preimage. It is helpful to visualize this construction not to scale. Figure 2·4 is a stylized depiction of the $\overline{0}\,TL$ arc in dynamical space. The arrow points to the fixed point in R_0^λ, so each successive preimage is a pair of smaller copies of L^λ and $T_\mathcal{A}$, and these preimages accumulate on the fixed point accessible from B_λ. Note that the compact containment as proved in Proposition 2.2.2 is not represented for the sake of avoiding visual clutter.

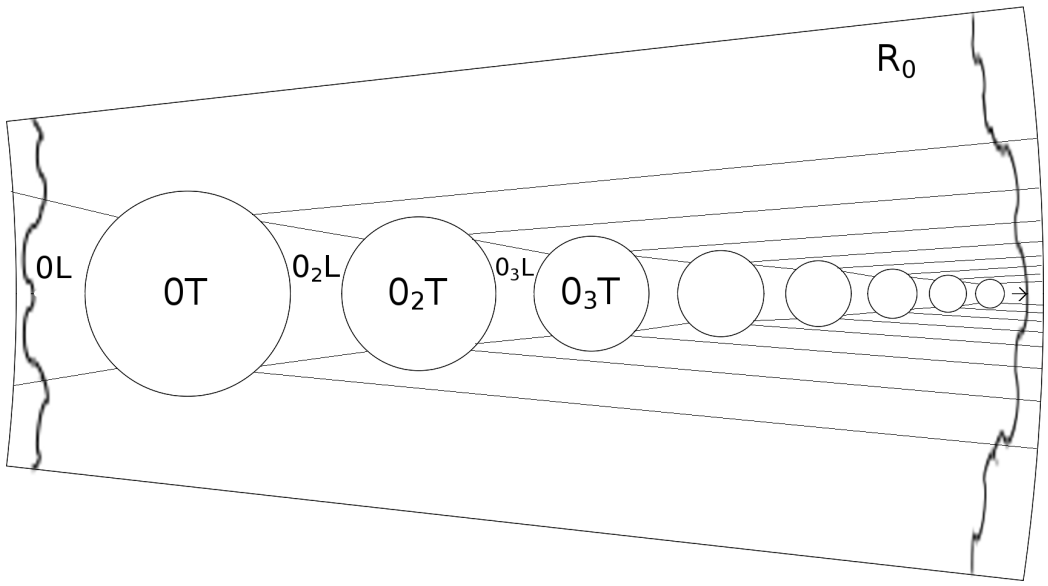

Figure 2·4: The $\overline{0}\,TL$ arc

Before we can use the existence of the $\overline{0}$ TL arc in R_0^λ to show the existence of a SM arc in the parameter plane, we recall the concept of a polynomial-like map. Let G_μ be a family of holomorphic maps that depends analytically on the parameter μ lying in some open disk $\mathcal{D}$. Suppose each $G_\mu : U_\mu \to V_\mu$ where both U_μ and V_μ are open disks that also depend analytically on μ. G_μ is then said to be polynomial-like of degree two if, for each μ:

- G_μ maps U_μ two-to-one onto V_μ and so there is a unique critical point in U_μ;
- V_μ contains U_μ;
- As μ winds once around the boundary of $\mathcal{D}$, the critical value winds once arond U_μ in the region $V_\mu - U_\mu$.

As shown in (Douady and Hubbard, 1985), for such a family of polynomial-like maps, there is a homeomorphic copy of the Mandelbrot set in the disk $\mathcal{D}$. Moreover, for μ-values in this Mandelbrot set, $G_\mu|U_\mu$ is conjugate to the corresponding quadratic map given by this homeomorphism.

We have an arc of infinitely many alternating preimages of L^λ and $T_\mathcal{A}$ in the dynamical space. We show that the center of each preimage of $T_\mathcal{A}$ is the critical value for a specific λ that is the center of a Sierpinski hole. Then we use the machinery of polynomial-like maps on some open sets to prove that each preimage of L^λ corresponds to a Mandelbrot set. Thus, the existence of a dynamical TL arc proves the existence of a corresponding parameter arc of infinitely many Sierpinski holes and Mandelbrot sets.

Theorem 2.3.1. *There exists the $\overline{0}$ SM arc along the negative real axis in the parameter plane that consists of infinitely many Mandelbrot sets $\mathcal{M}^k$ with $k \geq 2$ and infinitely many Sierpinski holes $\mathcal{E}^k$ with $k \geq 1$. Here k denotes the base period of $\mathcal{M}^k$*

and the escape time of $\mathcal{E}^k$. These sets are arranged along the negative real axis in this manner:

$$\text{Cantor set locus} < \cdots < \mathcal{M}^4 < \mathcal{E}^3 < \mathcal{M}^3 < \mathcal{E}^2 < \mathcal{M}^2 < \mathcal{E}^1.$$

Proof. We will first prove that each preimage of $T_{\mathcal{A}}$ in dynamical space corresponds to a Sierpinski hole in the parameter plane (the trap door itself corresponds to the McMullen domain). By construction, for each $\lambda \in \mathcal{S}_4 \bigcap \mathcal{O}$, there is a unique prepole p_3^λ in the interior of R_0^λ. Since F_λ maps R_0^λ one-to-one over itself, there is a unique preimage of this prepole, z_3^λ, in R_0^λ, so $F_\lambda^2(z_3^\lambda) = 0$. Continuing, for each $\lambda \in \mathcal{S}_4 \bigcap \mathcal{O}$, there is a unique point z_k^λ in R_0^λ for which we have $F_\lambda(z_k^\lambda) = z_{k-1}^\lambda$ and so $F_\lambda^{k-1}(z_k^\lambda) = 0$. This holds true for the $(k+1)^{st}$ case as well.

The points z_k^λ vary analytically with λ and are strictly contained in the interior of R_0^λ. So we may consider the function $H^k(\lambda)$ defined on $\mathcal{S}_4 \bigcap \mathcal{O}$ by $H^k(\lambda) = v_0^\lambda - z_k^\lambda$ where $v_0^\lambda = F_\lambda(c_0^\lambda)$. When λ rotates once around the boundary of $\mathcal{S}_4 \bigcap \mathcal{O}$, v_0^λ rotates once around the boundary of R_0^λ while z_k^λ remains in the interior of R_0^λ. Hence $H^k(\lambda)$ has winding number one around the boundary of $\mathcal{S}_4 \bigcap \mathcal{O}$ and so there must be a unique zero in $\mathcal{S}_4 \bigcap \mathcal{O}$ for each H^k. This λ is then the parameter that lies at the center of the escape time region $\mathcal{E}^k$. Using the technique from (Roesch, 2006), it then follows that $\mathcal{E}^k$ is an open disk in the parameter plane.

The λ in the parameter plane such that $v_0^\lambda = p_3^\lambda$ (with p_3^λ being the center of $0T$ in dynamical space) is the center of $\mathcal{E}^2$, so 2 is equivalently the escape time of c_0^λ for $\lambda \in \mathcal{E}^2$ and the length of the sequence $0T$.

The λ in the parameter plane such that $v_0^\lambda = z_3^\lambda$ (with z_3^λ being the center of $00T$ in dynamical space) is the center of $\mathcal{E}^3$, so 3 is equivalently the escape time of c_0^λ for $\lambda \in \mathcal{E}^3$ and the length of the sequence $00T$.

Continuing in this fashion, the λ in the parameter plane such that $v_0^\lambda = z_k^\lambda$ (with z_k^λ being the center of $0_{k-1}T$ in dynamical space) is the center of $\mathcal{E}^k$, so k is equivalently the escape time of c_0^λ for $\lambda \in \mathcal{E}^k$ and the length of the sequence $0_{k-1}T$.

Note that, as λ decreases along $\mathbb{R}^-$, both v_0^λ and z_k^λ increase along $\mathbb{R}^+$. It follows that the portion of $\mathcal{E}^{k+1}$ in $\mathbb{R}^-$ lies to the left of $\mathcal{E}^k$ in the parameter plane.

To prove the existence of the Mandelbrot sets $\mathcal{M}^k$, recall that the orbit of the point z_k^λ under F_λ remains in R_0^λ before entering $T_{\mathcal{A}}$ and landing at 0 at iteration $k-1$ (here $z_2^\lambda = p_3^\lambda$). For each $k \geq 2$, let E_λ^k be the open set surrounding z_k^λ in R_0^λ that is mapped onto $T_{\mathcal{A}}$ by F_λ^{k-1}. Let D_λ^k be the set in R_0^λ consisting of points whose

first $k-2$ iterations lie in R_0^λ but whose $(k-1)^{\text{st}}$ iterate lies in the interior of L^λ. Since F_λ is univalent on R_0^λ, each D_λ^k is an open disk. Furthermore, the boundary of D_λ^k meets a portion of the boundaries of both E_λ^{k-1} and E_λ^k (where $E_\lambda^1 = T_\mathcal{A}$). Since F_λ^{k-1} maps D_λ^k one-to-one over the interior of L^λ and then F_λ maps L^λ two-to-one over a region that contains R_0^λ, we have that F_λ^k maps D_λ^k two-to-one over a region that completely contains R_0^λ. Moreover, the critical value for F_λ^k is just v_0^λ, which, by the preceding Proposition, winds once around the exterior of R_0^λ as λ winds once around the boundary of $\mathcal{S}_4 \bigcap \mathcal{O}$. Hence, F_λ^k is a polynomial–like map of degree two on D_λ^k and this proves the existence of a baby Mandelbrot set $\mathcal{M}^k$ lying in $\mathcal{S}_4 \bigcap \mathcal{O}$ for each $k \geq 2$. When λ is real and negative, we have that the centers of the escape regions $\mathcal{E}^k$ lie along $\mathbb{R}^-$ and, since the real line is invariant under F_λ when $\lambda \in \mathbb{R}^-$, both c_0^λ and v_0^λ also lie on the real axis. Then, by the $\lambda \mapsto \overline{\lambda}$ symmetry in the parameter plane, the spines of those Mandelbrot sets also lie in $\mathbb{R}^-$. By the spine of the Mandelbrot set we mean the analogue of the portion of the real axis lying in the usual Mandelbrot set associated with the quadratic family $z^2 + c$.

Next, since the E_λ^k and D_λ^k are arranged along the TL arc from $T_\mathcal{A}$ out to the fixed point in the following fashion:

$$T_\mathcal{A} = E_\lambda^1 < D_\lambda^2 < E_\lambda^2 < D_\lambda^3 < E_\lambda^3 < \dots$$

we have that the $\mathcal{E}^k$ and $\mathcal{M}^k$ are arranged along the negative real axis in the parameter plane in the opposite manner:

$$\dots < \mathcal{M}^4 < \mathcal{E}^3 < \mathcal{M}^3 < \mathcal{E}^2 < \mathcal{M}^2 < \mathcal{E}^1$$

with the parameter passing alternately through the centers of infinitely many Sierpinski holes and along the spines of the same number of baby Mandelbrot sets.

Finally, when $\lambda \in \mathbb{R}^-$, there is a non-empty interval lying between each adjacent $\mathcal{M}^k$ and $\mathcal{E}^j$ (where $j = k$ or $k-1$). This interval contains parameters for which $F_\lambda^k(c_0^\lambda)$ lies in L^λ, but then $F_\lambda^{k+1}(c_0^\lambda)$ is back in R_0^λ and close to ∂B_λ. As a consequence, it takes more than k additional iterations for this critical orbit to reach $T_\mathcal{A}$ or return to L^λ.

□

Figure 2·5 shows the $\overline{0}$ SM arc. From right to left, we see the McMullen Domain, $\mathcal{E}^2$, $\mathcal{E}^3$, $\mathcal{E}^4$, and $\mathcal{E}^5$. $\mathcal{M}^2$ is visible between the McMullen domain and $\mathcal{E}^2$, but no other

$\mathcal{M}^k$ on the $\overline{0}$ SM arc can be seen at this scale. Between $\mathcal{E}^5$ and the Cantor set locus are infinitely more Sierpinski holes and Mandelbrot sets on the arc.

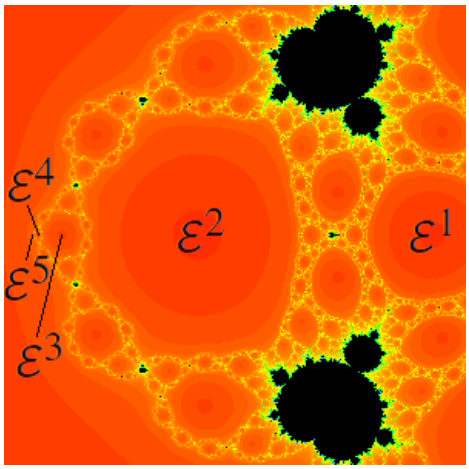

Figure 2·5: The $\overline{0}$ SM arc

Note that there are other Sierpinski holes and Mandelbrot sets along the arc that are not accounted for by the arc. Also, the arc contains infinitely many sets but is of finite length. One can find a Mandelbrot set or Sierpinski hole of arbitrarily high base period or escape time, but does so by zooming in as opposed to increasing $|\lambda|$.

2.4 Phase Three: The $\overline{1}$ TL Arc

Theorem 2.3.1 proves the existence of alternating Mandelbrot sets and Sierpinski holes along the negative real axis in the parameter plane by using the existence of alternating open sets E_λ^k and open disks D_λ^k, which correspond to the alternating preimages of $T_\mathcal{A}$ and L^λ along the positive real axis in the dynamical plane. This theorem also applies to the family $z^n + \lambda/z^d$ for $n \geq 2$ and even, and $d \geq 3$ and odd, and is detailed in (Devaney, 2016).

Recall that $F(R_0^\lambda) \supset R_0^\lambda$ (i.e. there is a preimage of R_0^λ inside R_0^λ), and so there is a fixed point inside R_0^λ accessible from B_λ. This preimage together with this fixed

point imply that successive preimages of the region that contains the interiors of L^λ, T_λ, and R_0^λ accumulate at the fixed point in R_0^λ. Recall that Proposition 2.2.2 refers to *two* right wedges, and according to that Proposition, there is a preimage of R_1^λ inside R_1^λ. Note that, since $F(R_1^\lambda) \supset R_1^\lambda$, there exists a unique fixed point in R_1^λ as well. However, this fixed point is "buried," i.e. not accessible from either B_λ or T_λ. One checks easily that this fixed point lies in the interior of R_1^λ.

This begs the question: is there an arc in R_1^λ analogous to the arc in R_0^λ? Is there a "$\overline{1}\ TL$ arc" of alternating preimages of L^λ and $T_\mathcal{A}$ that accumulate at the fixed point in R_1^λ?

In the proof of part 2 of Proposition 2.2.2, the outer boundary curve of R_1^λ is mapped to an arc to the *left* of the critical value rays in B_λ, while the inner boundary curve of R_1^λ is mapped to an arc to the *right* of the critical value rays. So the preimage of L^λ inside R_1^λ must be closer to B_λ while the preimages of R_0^λ and R_1^λ inside R_1^λ must be closer to T_λ. This is because the image of c_2^λ is p_{-3}^λ, and as z travels clockwise around the boundary of R_1^λ from c_{-3}^λ, $F_\lambda(z)$ travels clockwise around $\mathcal{A}$ from p_{-3}^λ. Thus the orientation remains the same for preimages of R_1^λ, and the set of preimages is rotated inside R_1^λ. This applies to all preimages for any number of iterations back. Thus, inside R_1^λ, each set of preimages that contains the interior of $R_0^\lambda \cup R_1^\lambda \cup L^\lambda$ is rotated in their corresponding preimage of R_1^λ.

In other words, the preimages in R_0^λ are arranged nicely in a straight line while the preimages in R_1^λ are arranged in a rotating pattern. Compare figures 2·6a and 2·6b.

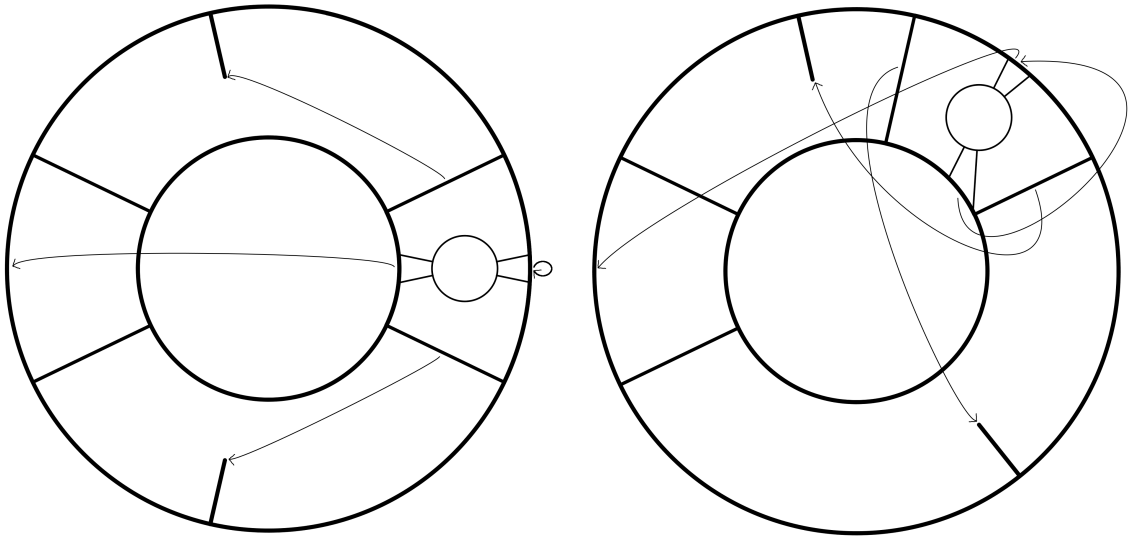

(a) The preimages in R_0^λ **(b)** The preimages in R_1^λ

Figure 2·6: Preimages inside R_0^λ vs R_1^λ

The $\overline{0}\,TL$ arc "grows" from T_λ and accumulates at the fixed point in R_0^λ accessible from B_λ. We use Proposition 2.2.2 to prove the existence of the $\overline{1}\,TL$ arc that "grows" from both B_λ and T_λ and accumulates at the buried fixed point in R_1^λ.

Inside R_1^λ there is a preimage of the region that contains the interior of $L^\lambda \cup T_\mathcal{A} \cup R_1^\lambda$. The prepole p_2^λ is inside the preimage of $T_\mathcal{A}$, so that we have the preimages of $R_1^\lambda \cup T_\mathcal{A} \cup L^\lambda$ in order along the arc, i.e. R_1^λ (which compactly contains the preimages of L^λ, $T_\mathcal{A}$, and R_1^λ), $T_\mathcal{A}$, then L^λ.

Using the itinerary naming scheme, there is T_λ, R_1^λ compactly containing $1R_1^\lambda, 1T_\mathcal{A}, 1L^\lambda$, then B_λ in order along the arc. Looking at the preimages inside $1R_1^\lambda$, we have T_λ, R_1^λ (compactly containing $1R_1^\lambda$ (compactly containing $1_2L^\lambda, 1_2T_\mathcal{A}, 1_2R_1^\lambda$)), $1T_\mathcal{A}, 1L^\lambda$, then B_λ. See figure 2·7.

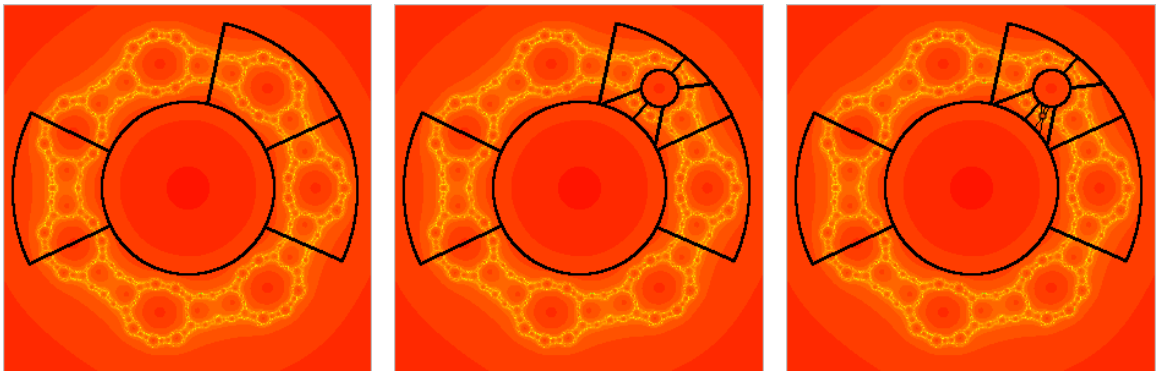

(a) The construction $L^\lambda, T_\mathcal{A}$, R_0^λ, and R_1^λ

(b) $1L^\lambda, 1T_\mathcal{A}$, $1R_0^\lambda$, and $1R_1^\lambda$ inside R_1^λ

(c) $1_2L^\lambda, 1_2T_\mathcal{A}$, $1_2R_0^\lambda$, and $1_2R_1^\lambda$ inside $1R_1^\lambda$

Figure 2·7: Preimages of the upper right wedge

This process continues iteratively as successive preimages of the region that contains the interiors of $L^\lambda, T_\mathcal{A}$, and R_1^λ meet in the middle, i.e., accumulate at the fixed point in the interior of R_1^λ. The preimages with an odd number of $1's$ in their name (i.e., even escape time or base period) are closer to B_λ, and the preimages with an even number of $1's$ in their name (i.e., odd escape time or base period) are closer to T_λ. As this arc consists of preimages named with only 1's that accumulate at the fixed point corresponding to the set with itinerary $111\ldots$, it is called the "$\overline{1}\ TL$ arc." This arc in dynamical space consists of infinitely many alternating preimages of L^λ and $T_\mathcal{A}$ between T_λ and B_λ:

$$T_\lambda, 1_2T_\mathcal{A}, 1_2L^\lambda, 1_4T_\mathcal{A}, 1_4L^\lambda, \ldots, \text{f.p. in } R_1^\lambda, \ldots, 1_3T_\mathcal{A}, 1_3L^\lambda, 1T_\mathcal{A}, 1L^\lambda, B^\lambda$$

Figure 2·8 is a depiction of the $\overline{1}\ TL$ arc in a style similar to the $\overline{0}\ TL$ arc. The X represents the fixed point in the interior of R_1^λ, so each successive preimage is a pair of smaller copies of L^λ and $T_\mathcal{A}$ on alternating sides of the X, and these preimages accumulate on the fixed point. Note that the fixed point is not accessible from B_λ or T_λ. Again, the compact containment is not represented.

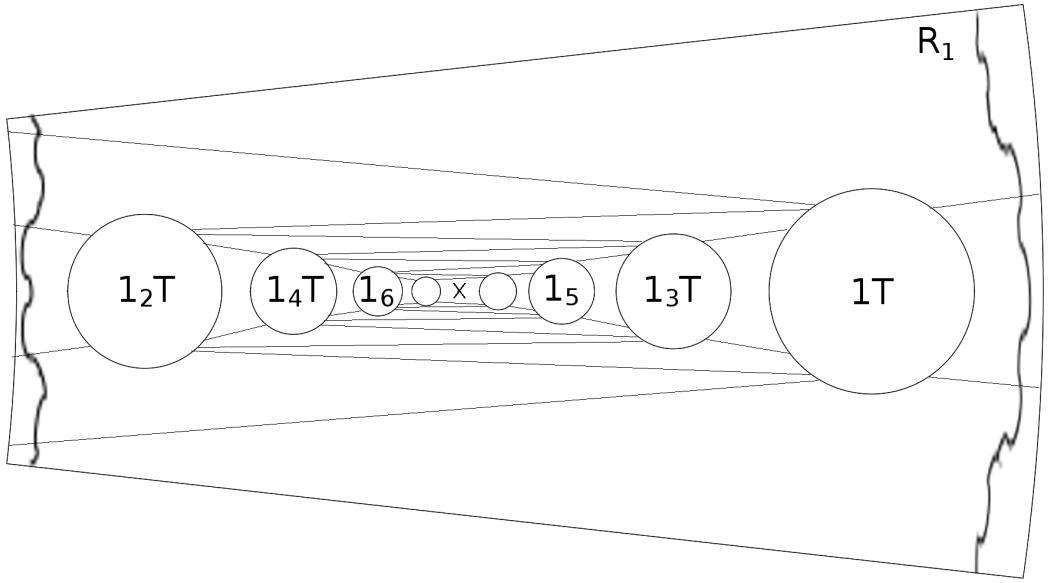

Figure 2·8: The $\overline{1}$ TL arc

2.5 Phase Four: The $\overline{1}$ TL Spiral

Up to this point, we have used Proposition 2.2.2 to find preimages of R_0^λ inside R_0^λ, and preimages of R_1^λ inside R_1^λ. In actuality, there is a preimage of the interiors of $L^\lambda \cup T_\mathcal{A} \cup R_0^\lambda \cup R_1^\lambda$ in R_0^λ, and a (rotated) preimage of the interiors of $L^\lambda \cup T_\mathcal{A} \cup R_0^\lambda \cup R_1^\lambda$ in R_1^λ. This means that the $\overline{0}$ TL arc, contained entirely inside R_0^λ, has a preimage contained entirely inside R_1^λ.

Consider the preimage of the $\overline{0}$ TL arc in R_1^λ: the $1\overline{0}$ TL arc. The $\overline{0}$ TL arc is arranged $T_\mathcal{A}, 0L^\lambda, 0T_\mathcal{A}, 0_2L^\lambda, 0_2T_\mathcal{A}, \ldots$ in order along the arc, or in order of increasing $|z|$. Therefore, it's preimage is arranged $1T_\mathcal{A}, 10L^\lambda, 10T_\mathcal{A}, 10_2L^\lambda, 10_2T_\mathcal{A}, \ldots$ in order along the arc. But the arc is rotated inside R_1^λ, so the sets are arranged in order of *decreasing* $|z|$.

The $1\overline{0}$ TL arc accumulates at the preimage of the fixed point. The fixed point is accessible from B_λ, therefore the preimage of the fixed point is accessible from T_λ. Due to the rotation of preimages inside R_1^λ, this preimage of the fixed point is above

the $\overline{1}\ TL$ arc, and so the entire $1\overline{0}\ TL$ arc is above the $\overline{1}\ TL$ arc.

Next, consider the preimage in R_1^λ of the $1\overline{0}\ TL$ arc. This is the $1_2\overline{0}\ TL$ arc, consisting of $1_2T_{\mathcal{A}}, 1_20L^\lambda, 1_20T_{\mathcal{A}}, 1_20_2L^\lambda, 1_20_2T_{\mathcal{A}}, \ldots$ in order along the arc. But the arc is rotated inside a rotated arc, i.e. the sets are arranged in order of *increasing* $|z|$. The $1_2\overline{0}\ TL$ arc accumulates at the preimage of the preimage of the fixed point. If the preimage of the fixed point is accessible from T_λ, the preimage of the preimage of the fixed point must not be accessible from either B_λ or T_λ. Due to the rotation of preimages inside R_1^λ, this preimage of the preimage of the fixed point is below the $\overline{1}\ TL$ arc, and so the entire $1_2\overline{0}\ TL$ arc exists below the $\overline{1}\ TL$ arc.

This process continues iteratively as successive preimages of the $\overline{0}\ TL$ arc, lying alternatingly above and below the $\overline{1}\ TL$ arc, limit to the preimage of the $\overline{0}\ TL$ arc such that the limit preimage arc and the $\overline{1}\ TL$ arc accumulate at the same fixed point in R_1^λ.

Figure 2·9 depicts the $\overline{1}\ TL$ spiral in dynamical space. A complex number z travels a continuous path that begins at the limit of the $1\overline{0}\ TL$ arc, along the $1\overline{0}\ TL$ to $1T_{\mathcal{A}}$, along the $1_2\overline{0}\ TL$ arc to $1_2T_{\mathcal{A}}$, along the $1_3\overline{0}\ TL$ arc to $1_3T_{\mathcal{A}}$, and so on, passing through every preimage of $T_{\mathcal{A}}$ in the $\overline{1}\ TL$ arc and limiting to the fixed point in R_1^λ. Note that z travels backward along each $1_k\overline{0}\ TL$ arc, or away from the limit z.

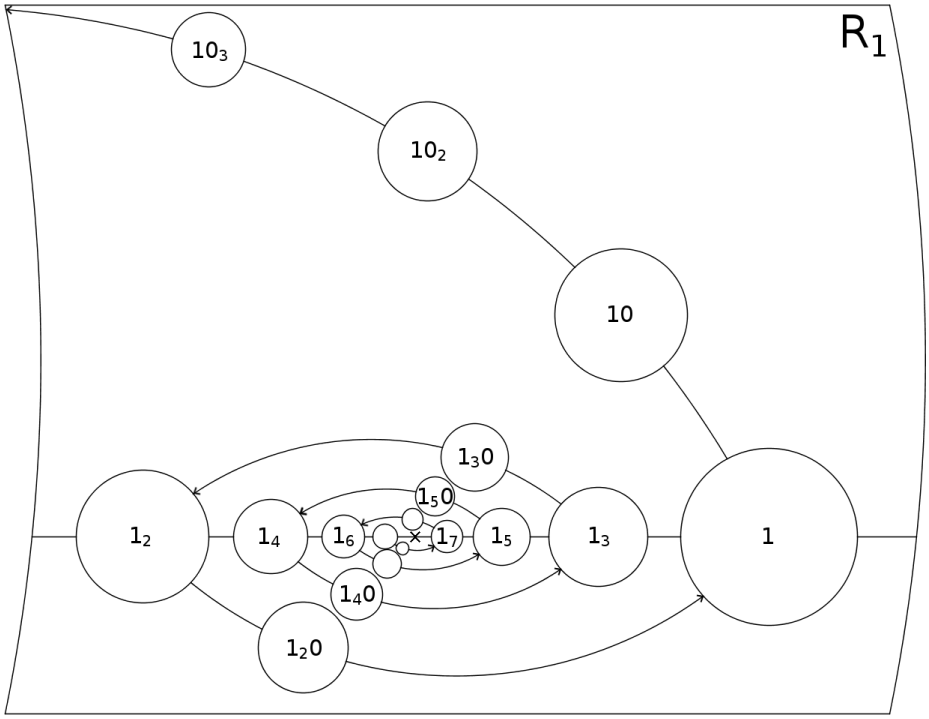

Figure 2·9: The $\overline{1}$ TL spiral

We have found a dynamical structure consisting of the $1\overline{0}$ TL arc and infinitely many of its preimages. Each sucessive preimage arc exists in a smaller and smaller region as the arcs tend to the limit arc in a spiral pattern. As this spiral passes through every $T_{\mathcal{A}}$ in the $\overline{1}$ TL arc, it is called the "$\overline{1}$ TL spiral." This spiral is an infinite sequence of arcs where each arc is itself an infinite sequence of pairs of preimages of L^{λ} and $T_{\mathcal{A}}$.

2.6 Phase Five: The $0\overline{1}$ SM Spiral

The $\overline{1}$ TL spiral in dynamical space consists of preimages of L^{λ} and $T_{\mathcal{A}}$. As each preimage of L^{λ} in dynamical space proves the existence of a Mandelbrot set in the parameter plane, and each preimage of $T_{\mathcal{A}}$ in dynamical space proves the existence of a Sierpinski hole in the parameter plane, the dynamical spiral suggests the existence

of a parameter spiral of Mandelbrot sets and Sierpinski holes. However, for all $\pi/3 <$ Arg $\lambda < 2\pi/3$, the critical value lies in R_0^λ. As a consequence, there are no such Mandelbrot sets or Sierpinski holes in the parameter plane that correspond to the preimages of $T_{\mathcal{A}}$ and L^λ in R_1^λ.

However, the $\overline{1}\ TL$ spiral is in R_1^λ, and there exists a preimage of R_1^λ inside R_0^λ. Therefore, we consider the $0\overline{1}\ TL$ spiral in dynamical space, and use that to prove the existence of the $0\overline{1}$ SM spiral in the parameter plane.

Theorem 2.6.1. *There exists a $0\overline{1}$ SM arc below the negative real axis in the parameter plane that consists of infinitely many Mandelbrot sets $\mathcal{M}^k$ and infinitely many Sierpinski holes $\mathcal{E}^k$ both with $k \geq 3$. As before, k denotes the base period of $\mathcal{M}^k$ and the escape time of $\mathcal{E}^k$. These sets are arranged in from the Cantor set locus to the McMullen domain in this manner:*

$$\text{Cantor set locus, } \mathcal{M}^3, \mathcal{E}^3, \mathcal{M}^5, \mathcal{E}^5, \mathcal{M}^7, \mathcal{E}^7, \ldots, \mathcal{E}^8, \mathcal{M}^8, \mathcal{E}^6, \mathcal{M}^6, \mathcal{E}^4, \mathcal{M}^4, \mathcal{E}^1.$$

Note that the Cantor set locus and the McMullen domain are not included in the $0\overline{1}$ arc.

Furthermore, there exists the $0\overline{1}$ SM spiral below the negative real axis in the parameter plane that spirals from the Cantor set locus along the $\overline{0}$ arc to the Sierpinski hole with itinerary $0T$, along the $01\overline{0}$ arc to the Sierpinski hole with itinerary $01T$, along the $01_2\overline{0}$ arc to the Sierpinski hole with itinerary 01_2T, along each $01_k\overline{0}$ arc to the Sierpinski hole with itinerary 01_kT, passing through each Sierpinski hole in the $0\overline{1}$ SM arc and limiting to the SM arc that accumulates at the parameter such that the critical value is the buried fixed point in R_1^λ.

Proof. We will again prove that each preimage of $T_{\mathcal{A}}$ in dynamical space corresponds to a Sierpinski hole in the parameter plane. By construction, for each $\lambda \in \mathcal{S}_4 \bigcap \mathcal{O}$, there is a unique prepole p_2^λ in the interior of R_1^λ. Since F_λ maps R_0^λ one-to-one onto a region containing the interior of R_1^λ, there is a unique preimage of this prepole, w_4^λ, in R_1^λ, so $F_\lambda^3(w_4^\lambda) = 0$. Continuing, for each $\lambda \in \mathcal{S}_4 \bigcap \mathcal{O}$, there is a unique point w_k^λ in R_0^λ for which we have $F_\lambda(w_k^\lambda) = w_{k-1}^\lambda$ and so $F_\lambda^{k-1}(w_k^\lambda) = 0$. This holds true for the $(k+1)^{st}$ case as well.

The points w_k^λ vary analytically with λ and are strictly contained in the interior of R_0^λ. So we may consider the function $H^k(\lambda)$ defined on $\mathcal{S}_4 \bigcap \mathcal{O}$ by $H^k(\lambda) = v_0^\lambda - w_k^\lambda$

where $v_0^\lambda = F_\lambda(c_0^\lambda)$. When λ rotates once around the boundary of $\mathcal{S}_4 \bigcap \mathcal{O}$, v_0^λ rotates once around the boundary of R_0^λ while w_k^λ remains in the interior of R_0^λ. Hence $H^k(\lambda)$ has winding number one around the boundary of $\mathcal{S}_4 \bigcap \mathcal{O}$ and so there must be a unique zero in $\mathcal{S}_4 \bigcap \mathcal{O}$ for each H^k. This λ is then the parameter that lies at the center of the escape time region $\mathcal{E}^k$. $\mathcal{E}^k$ is an open disk in the parameter plane.

The λ in the parameter plane such that $v_0^\lambda = w_3^\lambda$ (with w_3^λ being the center of $01T$ in dynamical space) is the center of $\mathcal{E}^3$, so 3 is equivalently the escape time of v_0^λ for $\lambda \in \mathcal{E}^3$ and the length of the sequence $01T_\mathcal{A}$. Under iteration by F_λ, $c_0^\lambda \in L^\lambda \to w_3^\lambda \in R_0^\lambda \to p_2^\lambda \in R_1^\lambda \to 0 \in T_\mathcal{A}$.

The λ in the parameter plane such that $v_0^\lambda = w_4^\lambda$ (with w_4^λ being the center of 01_2T in dynamical space) is the center of $\mathcal{E}^4$, so 4 is equivalently the escape time of v_0^λ for $\lambda \in \mathcal{E}^4$ and the length of the sequence $01_2T_\mathcal{A}$. Under iteration by F_λ, $c_0^\lambda \in L^\lambda \to w_4^\lambda \in R_0^\lambda \to w_3^\lambda \in R_0^\lambda \to p_2^\lambda \in R_1^\lambda \to 0 \in T_\mathcal{A}$.

Continuing in this fashion, the λ in the parameter plane such that $v_0^\lambda = w_k^\lambda$ (with w_k^λ being the center of $01_{k-2}T_\mathcal{A}$ in dynamical space) is the center of $\mathcal{E}^k$, so k is equivalently the escape time of v_0^λ for $\lambda \in \mathcal{E}^k$ and the length of the sequence $01_{k-2}T_\mathcal{A}$.

Note that, as k increases from an odd value to an even value, $|\lambda|$ decreases, while both $|v_0^\lambda|$ and $|w_k^\lambda|$ increase. As k increases from an even value to an odd value, $|\lambda|$ increases, while both $|v_0^\lambda|$ and $|w_k^\lambda|$ decrease. Successively higher odd values of k have lower $|\lambda|$ in the parameter plane and higher $|v_0^\lambda|$ and $|w_k^\lambda|$ in dynamical space, while successively higher even values of k have higher $|\lambda|$ in the parameter plane and lower $|v_0^\lambda|$ and $|w_k^\lambda|$ in dynamical space.

It follows that, in the parameter plane, in order of decreasing $|\lambda|$, the sets are arranged $\mathcal{E}^k, \mathcal{E}^{k+1}$ for k odd, $\mathcal{E}^{k+1}, \mathcal{E}^k$ for k even, with all odd escape time Sierpinski holes having higher center $|\lambda|$ than all even escape time Sierpinski holes.

To prove the existence of the Mandelbrot sets $\mathcal{M}^k$, recall that the point $w_k^\lambda \in R_0^\lambda$, has an orbit under F_λ in R_1^λ for iterates 1 through $k-2$, and enters T_λ at iteration $k-1$ (here $w_2^\lambda = p_2^\lambda$). For each $k \geq 3$, let E_λ^k be the open set surrounding w_k^λ in R_0^λ that is mapped onto T_λ by F_λ^{k-1}. Let D_λ^k be the set in R_0^λ consisting of points whose first $k-2$ iterates lie in R_1^λ but whose $(k-1)^{st}$ iterate lies in the interior of L^λ. Since F_λ is univalent on R_0^λ and R_1^λ, each D_λ^k is an open disk. Furthermore, the boundary of D_λ^k meets a portion of the boundaries of both E_λ^{k-2} and E_λ^k. Since F_λ^{k-1} maps D_λ^k one-to-one over the interior of L^λ and then F_λ maps L^λ two-to-one over a region that contains R_0^λ, we have that F_λ^k maps D_λ^k two-to-one over a region that completely contains R_0^λ. Moreover, the critical value for F_λ^k is just v_0^λ, which, by Proposition

2.2.2, winds once around the exterior of R_0^λ as λ winds once around the boundary of $\mathcal{S}_4 \bigcap \mathcal{O}$. Hence, F_λ^k is a polynomial-like map of degree two on D_k^λ and this proves the existence of a baby Mandelbrot set $\mathcal{M}^k$ lying in $\mathcal{S}_4 \bigcap \mathcal{O}$ for each $k \geq 3$.

□

As in the above proof, the center of each Sierpinski hole in the $0\overline{1}$ SM spiral can be calculated by solving $F^k(v^\lambda) = p_2^\lambda$, where p_2^λ is the prepole in R_1^λ and k corresponds to the escape time of the Sierpinski hole $\mathcal{E}^k$. They can also be verified by selecting λ in that Sierpinski hole and observing the itinerary of the critical value. A straightforward computation shows that the $01T_\mathcal{A}$ region corresponds to the 01 Sierpinski hole $\mathcal{E}^3$ located below the negative real axis in the parameter plane. The λ parameter value at the center of the 01 Sierpinski hole results in the map F^λ such that c_0^λ maps to v_0^λ inside $01T_\mathcal{A}$, which maps to $1T_\mathcal{A}$, which maps to exactly the center of the trap door (the origin). Similarly, the $01_2T_\mathcal{A}$ region, which is the preimage of the $01T_\mathcal{A}$ region, corresponds to the 01_2 Sierpinski hole $\mathcal{E}^4$. We adopt the convention of referring to the 01_2 Sierpinski hole as the "preimage" of the 01 Sierpinski hole because their corresponding regions in dynamical space have that relationship. We use the same convention for "preimage" SM arcs overall because their corresponding TL arcs have that relationship. For example, the $1_2\overline{0}$ TL arc is the preimage of the $1\overline{0}$ TL arc, so we refer to the $1_2\overline{0}$ SM arc as a "preimage" of the $1\overline{0}$ SM arc.

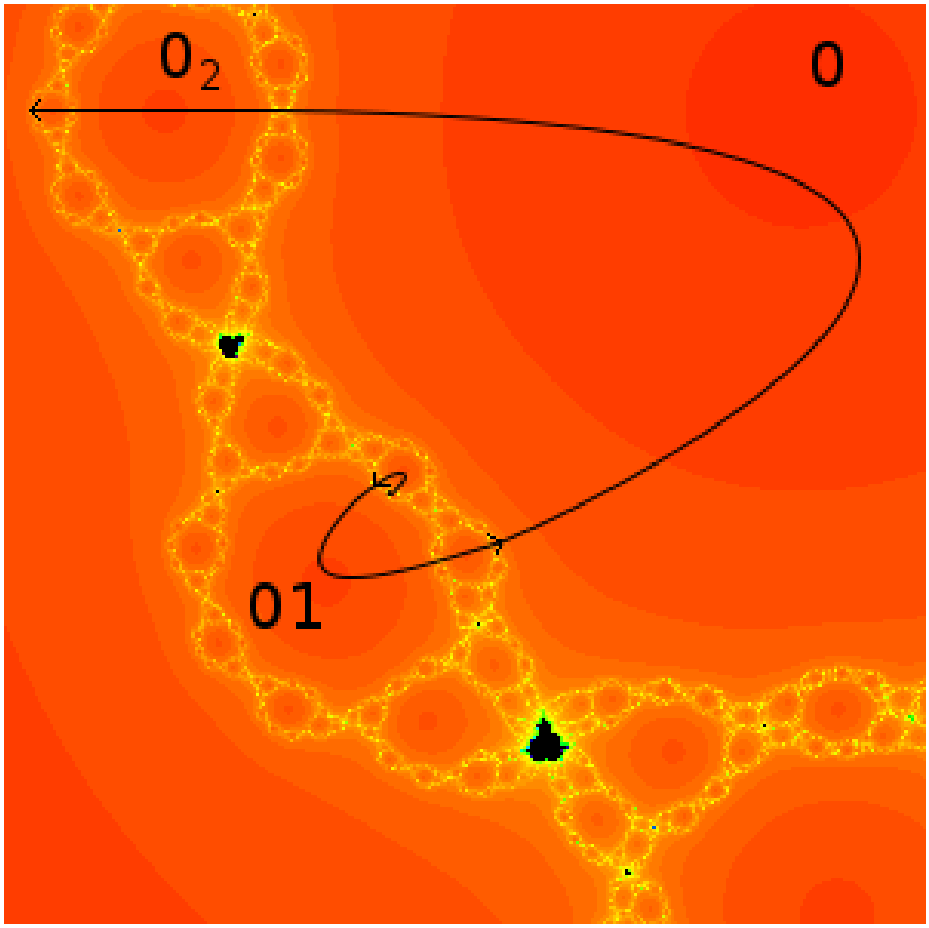

Figure 2·10: The $0\overline{1}$ SM spiral

Figure 2·10 shows the $0\overline{1}$ SM spiral as λ enters the connectedness locus from the Cantor set locus, travels along the $\overline{0}$ SM arc into the 0 Sierpinski hole, then along the $01\overline{0}$ arc into the 01 Sierpinski hole, then along the $01_2\overline{0}$ arc into the 01_2 Sierpinski hole, and so on. The 01_3 Sierpinski hole is a speck at this scale. Note that the arrows point to the accumulation points of the arcs (outward), while λ spirals inward.

2.7 Infinitely Many SM Spirals

In dynamical space, we have used Proposition 2.2.2 to find the preimage of the $\overline{1}$ spiral: the $0\overline{1}$ spiral in R_0^λ. This $0\overline{1}$ spiral has its preimage in R_0^λ, the $0_2\overline{1}$ spiral, and

its preimage in R_1^λ, the $10\overline{1}$ spiral. As expected, the $0_2\overline{1}$ spiral passes through every preimage of $T_\mathcal{A}$ in the $0_2\overline{1}$ arc, and the similar statement can be made about the $10\overline{1}$ spiral. The $0_2\overline{1}$ spiral has its preimages the $0_3\overline{1}$ arc and the $10_2\overline{1}$ spiral.

As for the $10\overline{1}$ spiral, its preimage in R_1^λ must pass through every preimage of $T_\mathcal{A}$ in the $1_20\overline{1}$ arc, is connected to $1_20T_\mathcal{A}$, which is part of the $1_2\overline{0}$ arc, which is part of the path of the $\overline{1}$ spiral. Its preimage in R_1^λ is connected to $010T_\mathcal{A}$ which is part of the $01\overline{0}$ arc.

It suffices to find the successive preimages in R_1^λ of the $0\overline{1}$ spiral to show that there are infinitely SM many spirals in the parameter plane of the form $0_k\overline{1}$. In dynamical space, we also find their preimages in R_1^λ, spirals of the form $10_k\overline{1}$, without difficulty.

If we take figure 2·9 and include the next three levels of preimages, we get figure 2·11. The preimages of the $\overline{1}$ TL spiral are itself and the $0\overline{1}$ TL spiral. The preimages of the $0\overline{1}$ TL spiral are the $0_2\overline{1}$ and $10\overline{1}$ TL spirals. The preimages of the $0_2\overline{1}$ TL spiral are the $0_3\overline{1}$ and $10_2\overline{1}$ TL spirals.

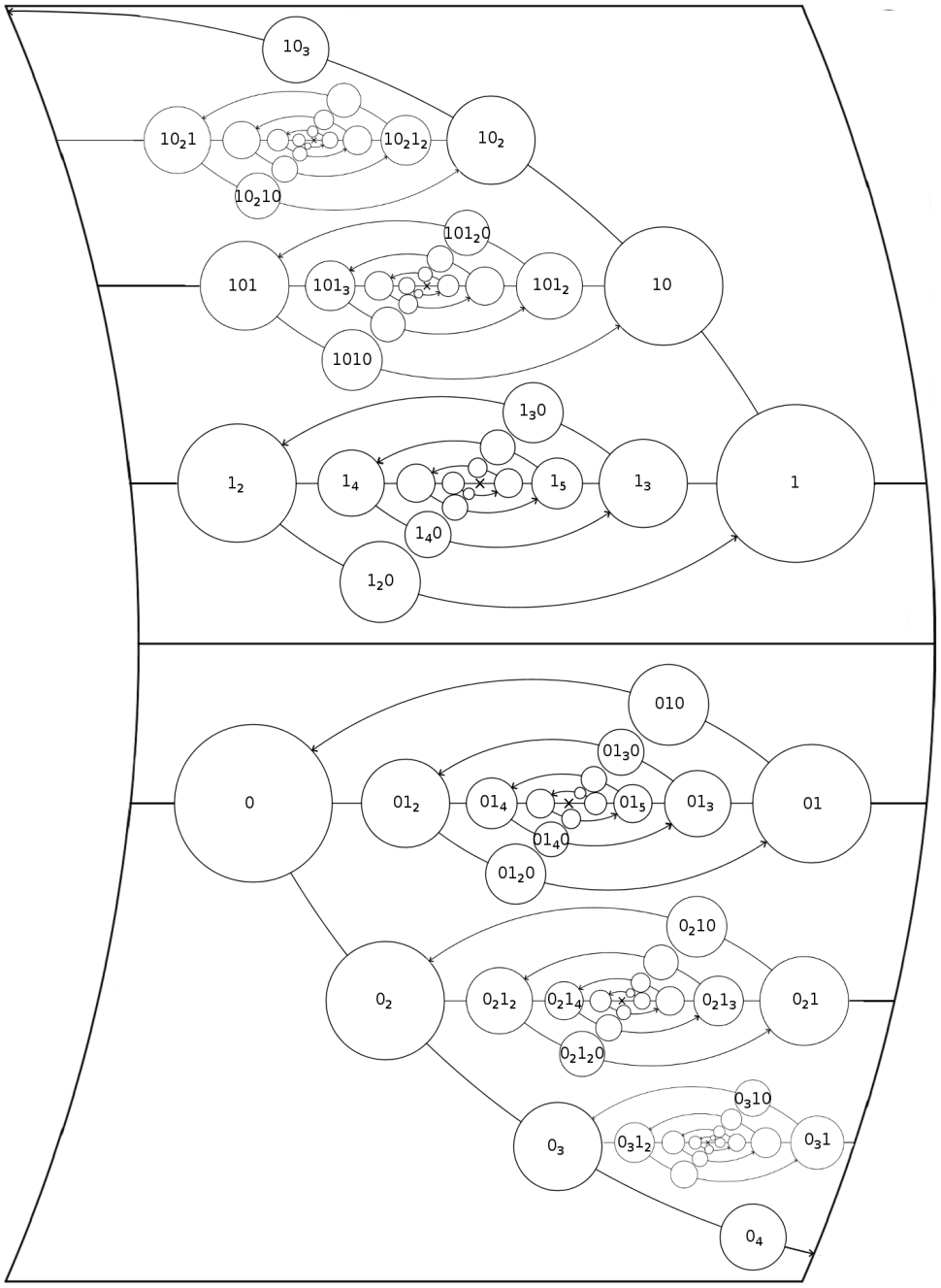

Figure 2·11: Infinitely many TL spirals

In parameter space, all SM spirals of the form $0_k\overline{1}$ can be found and verified as well. A more complete version of figure 2·10 including some of these infinitely many

spirals in the parameter plane would look like:

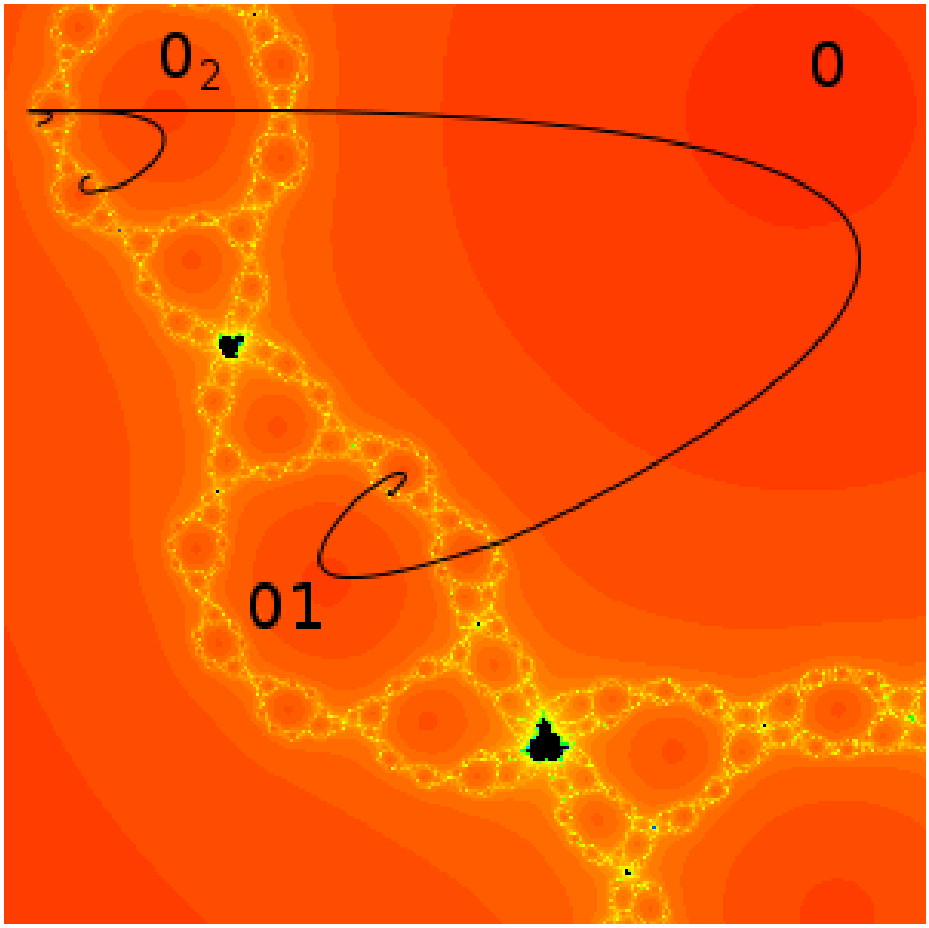

Figure 2·12: Infinitely many SM spirals

Figure 2·12 depicts the $0\overline{1}$ SM spiral as in figure 2·10, as well as its preimage the $0_2\overline{1}$ SM spiral, and the $0_2\overline{1}$ SM spiral's preimage the $0_3\overline{1}$ SM spiral. Whereas the $0\overline{1}$ SM spiral passes through the $\overline{0}$ SM arc to the 0 Sierpinski hole and then the $01\overline{0}$ SM arc, the $0_2\overline{1}$ SM spiral passes through the $\overline{0}$ SM arc to the 0_2 Sierpinski hole and then the $0_2\overline{1}$ SM arc.

We have shown that infinitely many SM spirals exist in the $\pi \leq \text{Arg } \lambda \leq 4\pi/3$ region of the parameter plane. However, the choice of R_1^λ being above R_0^λ was arbitrary. If we had chosen the other right wedge to be below R_0^λ - "the R_{-1}^λ wedge" - we

would have the symmetric "$\overline{-1}$" TL spiral in dynamical space and the corresponding counterclockwise "$0\overline{(-1)}$" SM spiral in the parameter plane, along with their infinitely many preimages.

Furthermore, by the threefold symmetry of the parameter plane, symmetric copies of these infinitely many spirals also exist in the $0 \leq \text{Arg } \lambda \leq 2\pi/3$ and $4\pi/3 \leq \text{Arg } \lambda \leq 2\pi$ regions of the parameter plane. Together with the lower wedge argument, for each spiral in the $\pi \leq \text{Arg } \lambda \leq 4\pi/3$ region of the parameter plane, there are actually six spirals in the parameter plane, as in figure 2·13. The collection of all of the SM spirals in the parameter plane is called the "SM hydra" because bouquet is taken, and because it sounds cool.

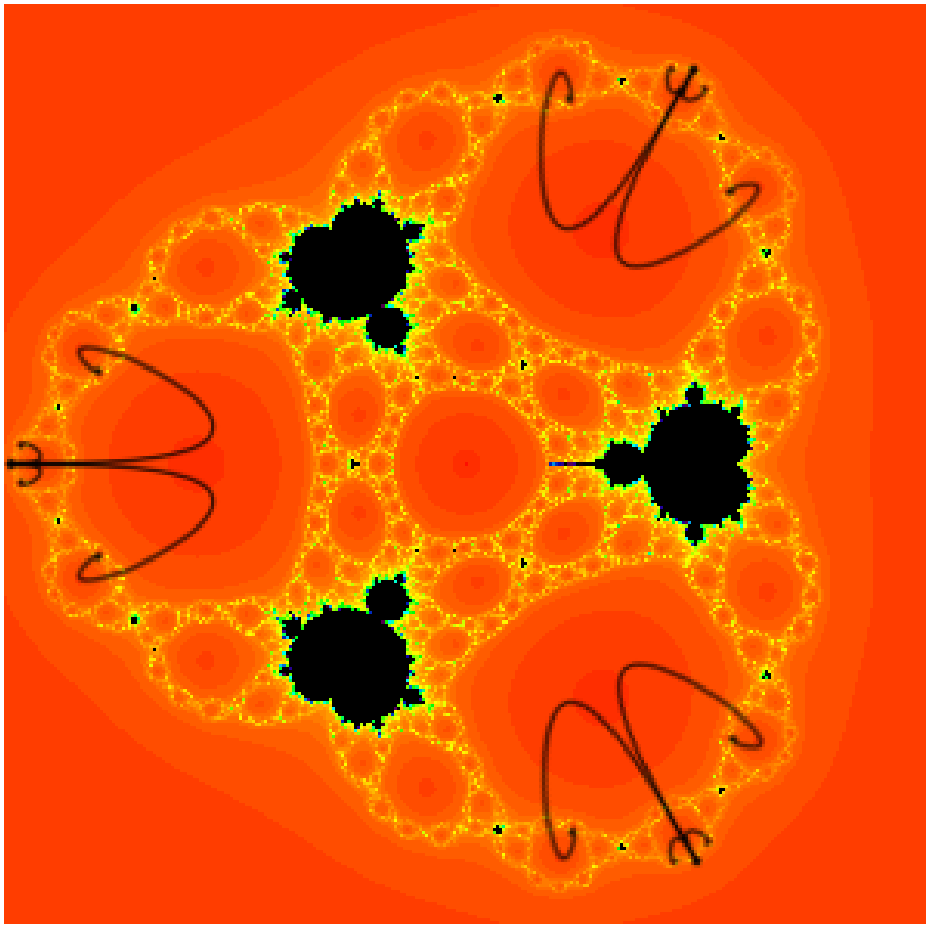

Figure 2·13: Here Are Infinite spiraLs comprising the SM Hydra

Chapter 3

The General Case

3.1 Overview

We extend the construction of the bowtie beyond $z^4+\lambda/z^3$ to more general $z^n+\lambda/z^d$. We then prove that the same properties about this analogous bowtie hold in an analogous sector of the parameter plane for almost all pairs of (n,d). The proof of Proposition 2.2.2 involved the specific angles of the dynamical rays, but there is a more elegant method for proving compact containment in the general case.

Given that a general Proposition 2.2.2 still holds for a general bowtie, the existence of general parameter structures follows. We then consider the pairs of (n,d) for which we can not prove a general Proposition 2.2.2, and find alternatives to the upper right wedge for almost all of the exceptional cases. This results in alternative or exceptional bowties, out of which we construct corresponding TL arcs, which prove the existence of corresponding SM arcs and spirals.

We widen our focus to the general case

$$F_\lambda(z) = z^n + \frac{\lambda}{z^d}$$

where $z \in \mathbb{C}$, $\lambda \in \mathbb{C}$ is nonzero, and $(n,d) \in \mathcal{D}$. $\mathcal{D}$ is defined to be the set of integer pairs (n,d) such that $n \geq 4$ is even and $d \geq 3$ is odd. Please don't confuse this $\mathcal{D}$ with the open disk in the context of polynomial-like maps.

There is $(n-1)$fold symmetry in the parameter plane for these maps, and $n-1$

principal Mandelbrot sets in the parameter plane whose spines lie along the rays that pass through the $(n-1)^{th}$ roots of unity. As n increases, we need only be concerned with smaller sectors of the parameter plane. Figure 3·3a shows the parameter plane for $z^{10} + \lambda/z^7$ with ninefold symmetry.

As in section 1.2, there are $n + d$ critical points, critical values, and prepoles. In the $(10, 7)$ case, the 17fold symmetry is apparent in figure 3·3b.

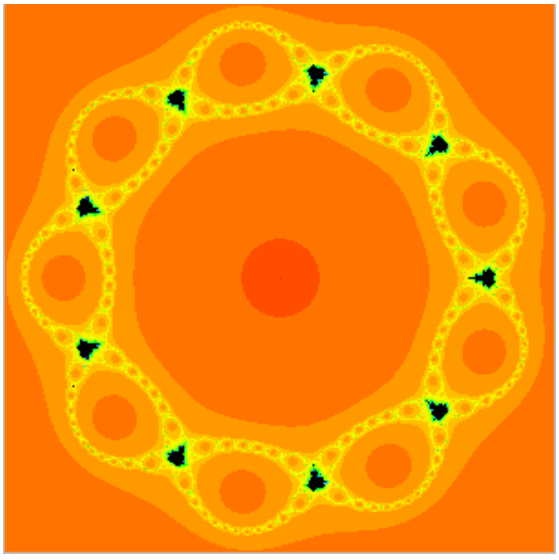

(a) The parameter plane for $z^{10} + \lambda/z^7$

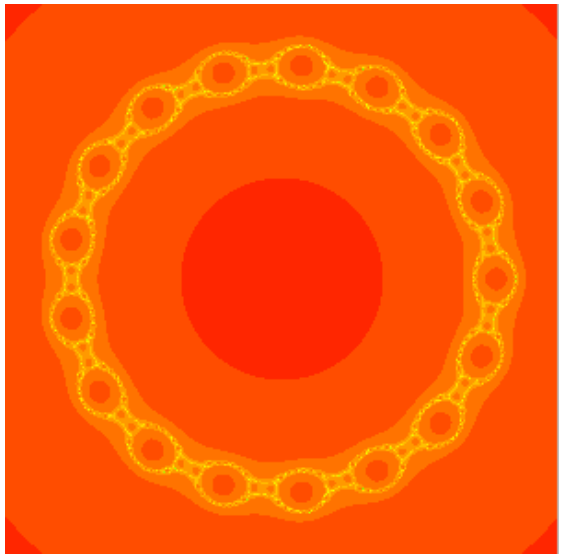

(b) The dynamical space for $z^{10}+\lambda/z^7$ with λ in a Sierpinski hole

Figure 3·1: Parameter and dynamical planes for $z^{10} + \lambda/z^7$

3.2 The General Bowtie Construction

We require a general Proposition 2.2.1. As in section 2.3, we may find constants $\alpha < 1$ and $\beta > 1$ such that, for $\lambda \in \mathcal{S}_n$ and $|\lambda| = \alpha$, then λ lies in the McMullen domain, whereas if $|\lambda| = \beta$, then λ lies in the Cantor set locus. Furthermore, we may construct an annulus $\mathcal{A}$ in the dynamical plane that encircles the origin and has the property that, if $|\lambda| = \alpha$, then v_0^λ lies on the inner circular boundary of $\mathcal{A}$, whereas if $|\lambda| = \beta$, then v_0^λ lies on the outer circular boundary of $\mathcal{A}$. Just as in Proposition

2.2.1, we may arrange that, if $\alpha < |\lambda| < \beta$, then F_λ maps both the inner and outer boundary of $\mathcal{A}$ strictly outside $\mathcal{A}$. We then define the region $\mathcal{O}$ in the parameter plane to be the set of λ that satisfy $\alpha \leq |\lambda| \leq \beta$.

Due to the $(n-1)$fold symmetry, we need only look at λ in $\mathcal{S}_n$ given by $\frac{n-2}{2(n-1)}2\pi \leq \text{Arg}\lambda \leq \frac{n}{2(n-1)}2\pi$. Altogether, we restrict attention to the region $\mathcal{S}_n \bigcap \mathcal{O}$.

We now define the general sectors L^λ, R_0^λ, R_1^λ, and $T_\mathcal{A}$ in dynamical space when $\lambda \in \mathcal{S}_n \bigcap \mathcal{O}$. First, when $\lambda \in \mathbb{R}^-$, L^λ is the region contained in the annulus $\mathcal{A}$ and bounded by the two prepole rays given by

$$\frac{\text{Arg } z}{2\pi} = \frac{1}{2} \pm \frac{1}{2(n+d)}.$$

R_0^λ is contained in $\mathcal{A}$ and is bounded by the two critical point rays given by

$$\frac{\text{Arg } z}{2\pi} = \pm\frac{1}{2(n+d)}.$$

R_1^λ is contained in $\mathcal{A}$ and is bounded by the two critical point rays given by

$$\frac{\text{Arg } z}{2\pi} = \frac{2}{2(n+d)} \pm \frac{1}{2(n+d)}.$$

$T_\mathcal{A}$ is the open portion of the trap door bounded by $\mathcal{A}$.

As λ rotates through $\mathcal{S}_n \bigcap \mathcal{O}$ in the clockwise direction by $\frac{1}{2(n-1)}$ of a turn, the critical points and prepoles on the straightline boundaries of these sectors each rotate by $\frac{1}{2(n-1)(n+d)}$ of a turn in the clockwise direction. The images of the critical point rays rotate by $\frac{n}{2(n-1)(n+d)}$ of a turn in the clockwise direction. The statement still holds if we replace clockwise with counter-clockwise. In effect, higher n results in the critical value rays rotating relatively more compared to the critical point or prepole rays. This is balanced by the fact that we need only consider λ in a smaller $\mathcal{S}_n$.

Proposition 3.2.1. *For $z^n + \lambda/z^d$ where $(n, d) \in \mathcal{D}$, when rotating λ by $\frac{1}{2(n-1)}$ of*

a turn, so long as a critical value ray does not land inside or on the boundary of a wedge for $\lambda \in \mathcal{R}^-$, that critical value ray can catch up to - but not pass - the critical point boundary of the wedge.

Proof. If a ray does not land inside or on the boundary of a wedge, then the difference in their arguments is at least $\left(\frac{1}{2(n+d)}\right) 2\pi$. After rotating $\frac{1}{n-1}$ of a turn (i.e. $\frac{1}{n-1}\pi$), the critical point ray has rotated $\frac{1}{n-1}\left(\frac{1}{2(n+d)}\right) 2\pi$, while the critical value ray has rotated $\frac{n}{n-1}\left(\frac{1}{2(n+d)}\right) 2\pi$.

They rotate with the same orientation, so the critical value ray is

$$\left(\frac{n}{n-1} - \frac{1}{n-1}\right)\left(\frac{1}{2(n+d)}\right) 2\pi = \left(\frac{n-1}{(n-1)(2)(n+d)}\right) 2\pi = \left(\frac{1}{(2)(n+d)}\right) 2\pi$$

closer to the critical point ray in argument. Therefore, a critical value ray that is not already inside or on the boundary of a wedge can at most be on the critical point boundary of a wedge. □

The critical value rays from R_0^λ never land inside or on the boundary of a wedge. This is established in (Devaney, 2016) for the left and right wedges. We must also check that the rays do not land in R_1^λ. The lower boundary critical point ray of R_1^λ is the same as the upper boundary critical point ray of R_0^λ, so that has been covered. It remains to verify that the image of the upper boundary critical point ray of R_1^λ satisfies the hypothesis of 3.2.1. However, this ray can cause problems.

Proposition 3.2.2. *For $z^n + \lambda/z^d$ where $(n, d) \in \mathcal{D}$,*
1. The images of the critical point rays bounding R_0^λ never land inside or on the boundary of L^λ or R_0^λ;
2. The image of the upper boundary critical point ray of R_0^λ does not land inside or on the boundary of L^λ or R_0^λ except for (n, d) such that:
i. $n = 2d$;
ii. $n = 2(d + 1)$;
iii. $n = \frac{d+1}{2}$;
iv. $n = \frac{d-1}{2}$.

Proof. For the first part, the lower critical point ray bounding R_0^λ at Arg $z = \frac{-1}{2(n+d)}2\pi$ is sent to $\frac{-n}{2(n+d)}2\pi = \frac{2(n+d)-n}{2(n+d)}2\pi$.

$$\frac{1}{2} + \frac{1}{2(n+d)} = \frac{n+d+1}{2(n+d)} < \frac{2(n+d)-n}{2(n+d)} = \frac{n+2d}{2(n+d)} < \frac{-1}{2(n+d)} = \frac{2n+2d-1}{2(n+d)}$$

for $(n,d) \in \mathcal{D}$, i.e., the lower critical value ray always lands between L^λ and R_0^λ.

The upper critical point ray bounding R_0^λ at Arg $z = \frac{1}{2(n+d)}2\pi$ is sent to $\frac{n}{2(n+d)}2\pi$.

$$\frac{3}{2(n+d)} < \frac{n}{2(n+d)} < \frac{1}{2} - \frac{1}{2(n+d)} = \frac{n+d-1}{2(n+d)}$$

for $(n,d) \in \mathcal{D}$, i.e., the lower critical value ray always has argument between R_1^λ and L^λ.

For the second part, the upper critical point ray bounding R_1^λ does not behave as nicely under iteration by F_λ. As n is even, the critical value ray can only land inside R_0^λ or R_1^λ, or on the boundary of L^λ. This critical value ray has Arg $z = \frac{3n}{2(n+d)}2\pi \in (0, 4\pi)$. We consider all ways the ray can land such that the hypothesis of Proposition 3.2.1 is not satisfied:

i. Inside $R_0^\lambda \implies 3n - 2(n+d) = 0 \implies n = 2d$.

ii. Inside $R_1^\lambda \implies 3n - 2(n+d) = 2 \implies n = 2d+2$.

iii. Upper boundary of $L^\lambda \implies 3n = n+d-1 \implies 2n = d-1$.

iv. Lower boundary of $L^\lambda \implies 3n = n+d+1 \implies 2n = d+1$.

□

We denote the set of $(n,d) \in \mathcal{D}$ for which Proposition 3.2.1 does not apply by $\mathcal{C}$. Please note that this is distinct from the Cantor set locus in the parameter plane.

$$\mathcal{C} = \{(n,d) \in \mathcal{D} \text{ such that } n = 2d, n = 2(d+1), \text{ or } 2n = d \pm 1\}$$

3.3 General Arcs and Spirals

For $(n,d) \in \mathcal{D} \setminus \mathcal{C}$, we have a general Proposition 2.2.1 and a general bowtie for which a general Proposition 2.2.2 applies in a general subset $\mathcal{S}_n \bigcap \mathcal{O}$ of the parameter plane. Then the process of constructing the $\overline{0}\ TL$ arc, the $\overline{1}\ TL$ arc, the $\overline{1}\ TL$ spiral, the $0\overline{1}$

TL spiral, and the $0\overline{1}$ SM spiral goes over essentially without change for this general case.

3.4 Alternative Wedges and Exceptional Spirals

There are four possible cases in which the image of the upper boundary critical point ray of R_1^λ can break the bowtie construction. For each case, we present an alternative upper right wedge R_k^λ such that the compact containment of Proposition 2.2.2 holds.

3.4.1 $n = 2d$

$z^6 + \lambda/z^3$ is the first pair of $(n, d) \in \mathcal{D}$ such that $n = 2d$. The image of the critical point ray at Arg $z = \frac{3}{18}2\pi$ has Arg $z = 0$ and is in R_0^λ, so R_1^λ does not compactly contain the bowtie. The next upper right wedge, R_2^λ, shares the problematic critical point boundary ray with R_1^λ, so it does not compactly contain $L^\lambda \cup T_\mathcal{A} \cup R_0^\lambda \cup R_2^\lambda$. The next upper right wedge, R_3^λ, with critical point boundary rays at Arg $z = \frac{5}{18}2\pi$ and $\frac{7}{18}2\pi$, has farther critical value ray at Arg $z = 6\left(\frac{7}{18}2\pi\right) \equiv \frac{6}{18}2\pi$, which is inside R_3^λ, so it does not compactly contain $L^\lambda \cup T_\mathcal{A} \cup R_0^\lambda \cup R_3^\lambda$, as seen in figure 3·2. There are no more possibilities as R_4^λ would overlap with L^λ, and the lower wedges behave symmetrically.

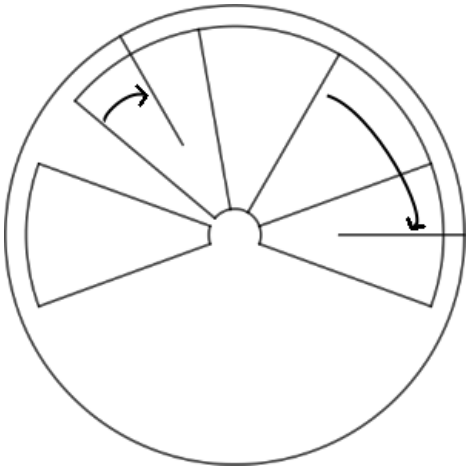

Figure 3·2: No workable alternative upper right wedge

$z^{10} + \lambda/z^5$ is the next pair in $\mathcal{C}$ such that the image of R_1^λ lands in R_0^λ. The alternative upper right wedge R_3^λ has critical value rays at Arg $z = 10\left(\frac{5}{30}2\pi\right) \equiv \frac{20}{30}2\pi$ and Arg $z = 10\left(\frac{7}{30}2\pi\right) \equiv \frac{10}{30}2\pi$. This bowtie consisting of $L^\lambda \cup T_\mathcal{A} \cup R_0^\lambda \cup R_3^\lambda$ (instead of R_0^λ) satisfies an analogous Proposition 2.2.2.

The alternative upper right wedge R_3^λ has closer critical value ray at Arg $z = n\left(\frac{5}{2(n+d)}2\pi\right) = \frac{10d}{6d}2\pi \equiv \frac{4d}{6d}2\pi$. As $d \geq 5$, this critical value ray at Arg $\frac{z}{2\pi} = \frac{4d}{6d}$ is between the lower L^λ ray at $\frac{3d+1}{6d}$ and the lower R_0^λ ray $\frac{6d-1}{6d}$.

The wedge has farther critical value ray at Arg $z = n\left(\frac{7}{2(n+d)}2\pi\right) = \frac{14d}{6d}2\pi \equiv \frac{2d}{6d}2\pi$. As $d \geq 5$, this critical value ray at Arg $\frac{z}{2\pi} = \frac{2d}{6d}$ is between the farther R_3^λ ray at $\frac{7}{6d}$ and the upper L^λ ray $\frac{3d-1}{6d}$. Figure 3·3 illustrates how the critical value rays do not move while the wedges themselves decrease in size.

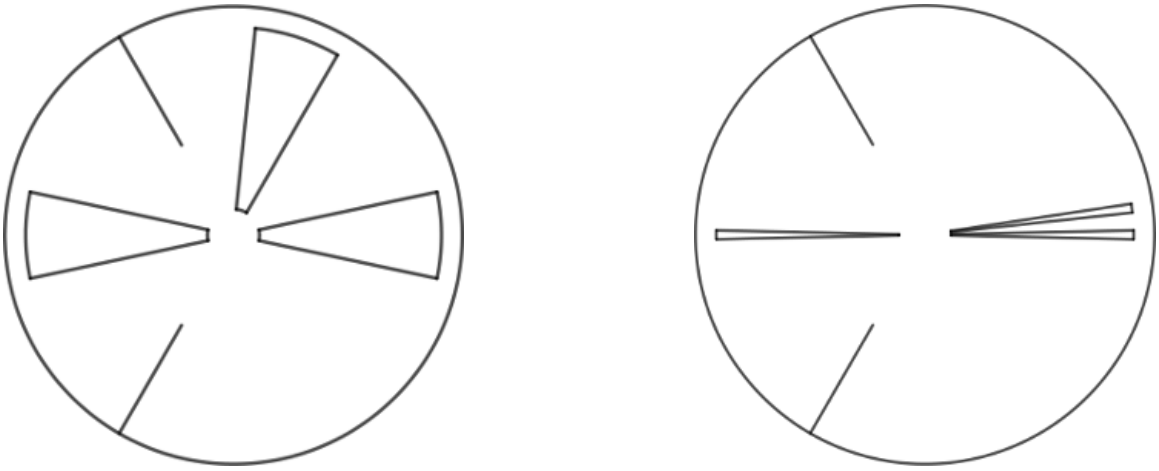

(a) The R_3^λ bowtie for $z^{10} + \lambda/z^5$ **(b)** The R_3^λ bowtie for $z^{98} + \lambda/z^{49}$

Figure 3·3: The exceptional R_3^λ bowtie construction

For all (n, d) such that $n = 2d$ except for $(6, 3)$, this exceptional bowtie leads to the $\overline{0}$ TL arc and the *exceptional*$\overline{3}$ TL arc. Together, those arcs comprise the exceptional $\overline{3}$ TL spiral, its preimage the exceptional $0\overline{3}$ TL spiral, and its corresponding exceptional "$0\overline{3}$ SM spiral" in the parameter plane.

3.4.2 $n = 2(d + 1)$

For $n = 2(d + 1)$, the bowtie consisting of $L^\lambda, T_\mathcal{A}, R_0^\lambda$, and alternative upper right wedge R_7^λ satisfies an analogous Proposition 2.2.2 for all cases but $(8, 3)$. R_7^λ has critical point rays at Arg $z = \frac{13}{2(n+d)}2\pi$ and $\frac{15}{2(n+d)}2\pi$, and it is relatively simple to check that these rays satisfy Proposition 3.2.1. From there the process of constructing the exceptional $0\overline{7}$ SM spiral goes over essentially without change.

For $(8, 3)$, the particular choice of R_8^λ suffices to construct the exceptional $0\overline{8}$ SM spiral. Note that this choice is less broadly applicable compared to R_7^λ.

3.4.3 $2n = d - 1$

For $2n = d-1$, the bowtie consisting of $L^\lambda, T_\mathcal{A}, R_0^\lambda$, and alternative upper right wedge R_5^λ satisfies an analogous Proposition 2.2.2 for all cases but $(4, 7)$. R_5^λ has critical point rays at Arg $z = \frac{9}{2(n+d)}2\pi$ and $\frac{11}{2(n+d)}2\pi$, and it is relatively simple to check that these rays satisfy Proposition 3.2.1. From there the process of constructing the exceptional $0\overline{5}$ SM spiral goes over essentially without change.

For $(4, 7)$, there is no possible choice of upper right wedge that satisfies Proposition 3.2.1.

3.4.4 $2n = d + 1$

For $2n = d+1$, the bowtie consisting of $L^\lambda, T_\mathcal{A}, R_0^\lambda$, and alternative upper right wedge R_3^λ again satisfies an analogous Proposition 2.2.2, for all cases but $(4, 9)$.

For $(4, 9)$, the particular choice of R_4^λ suffices to construct the exceptional $0\overline{4}$ SM spiral. Note that this choice is less broadly applicable compared to R_3^λ.

We have shown that a $0\overline{1}$ SM spiral exists for the family of rational maps $z^n+\lambda/z^d$ for all $(n, d) \in \mathcal{D} \setminus \mathcal{C}$. We have found exceptional - $0\overline{3}$, $0\overline{4}$, $0\overline{5}$, $0\overline{7}$, $0\overline{8}$ - SM spirals for all $(n, d) \in \mathcal{C}$ except for the two cases $(6, 3)$ and $(4, 7)$. In fact, the search for alternative upper right wedges led to the discovery that more than one type of spiral can exist for a given (n, d).

3.5 The $\overline{2}$ TL and SM arcs

It should be noted that all of the exceptional spirals mentioned up to this point are spirals only in the sense that they are analogues of the $0\overline{1}$ spiral. These exceptions motivated the construction of alternative wedges and the consequent arc and spirals, but are not a requirement. $z^n + \lambda/z^d$ with (n, d) such that the $0\overline{1}$ SM spiral provably

exists can have alternative spirals as well. To get a sense of their structure, we consider $z^4 + \lambda/z^5$, noting that R_2^λ satisfies 3.2.1, and therefore both the $\overline{1}$ TL arc and alternative $\overline{2}\ TL$ arc exist in dynamical space.

Figure 3·4 depicts a typical dynamical space and the R_2^λ bowtie, its preimage, and the preimage of its preimage.

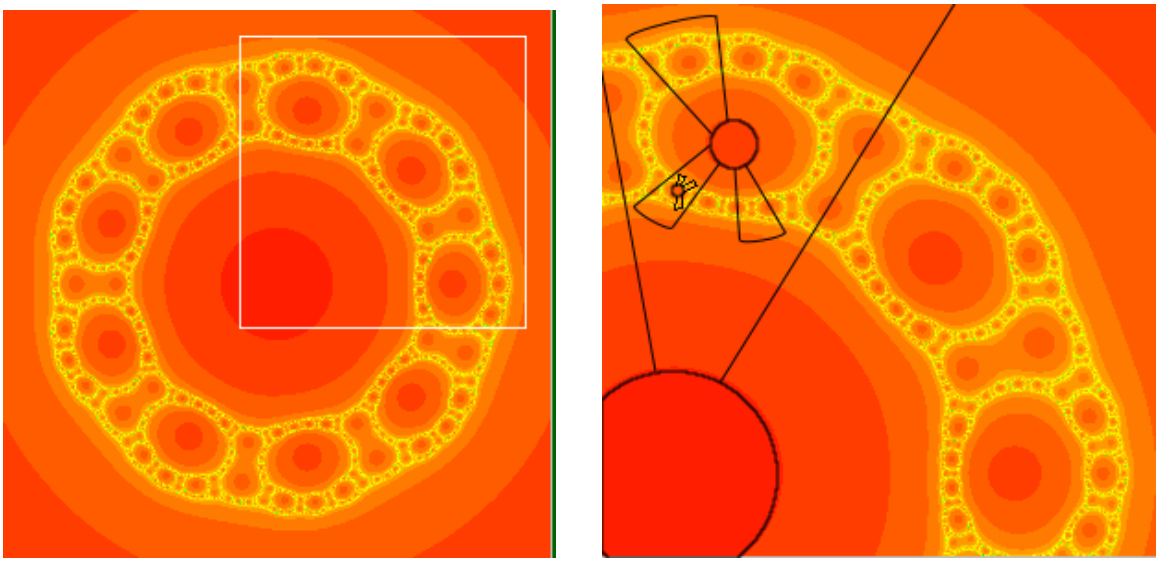

(a) The dynamical space for $z^4 + -0.88/z^5$

(b) The preimage of the preimage of the R_2^λ bowtie

Figure 3·4: The $\overline{2}\ TL$ arc

Figure 3·5 depicts the parameter plane and shows the $02, 02_2$, and 02_3 Sierpinski holes connected by line segments that are part of the $0\overline{2}$ SM arc.

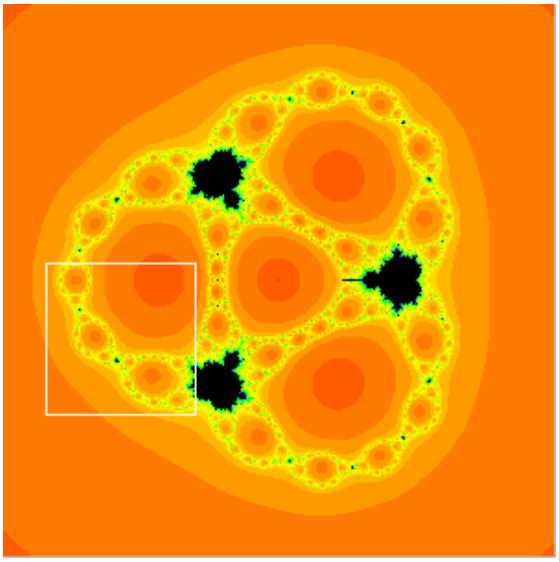

(a) The parameter plane for $z^4 + \lambda/z^5$

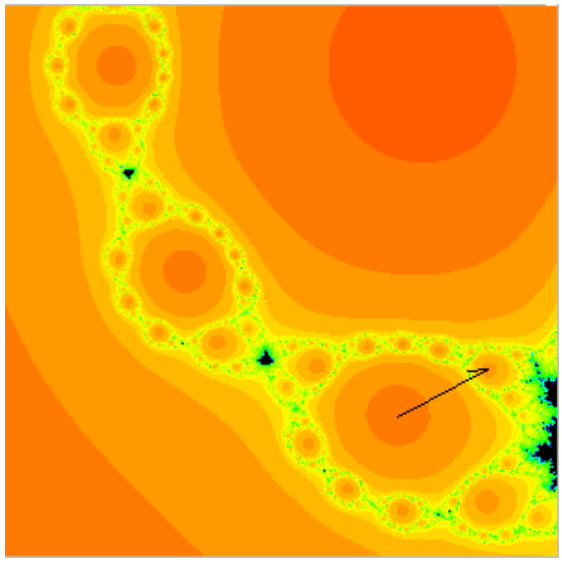

(b) The three Sierpinski holes in the $0\overline{2}$ SM arc with lowest escape time

Figure 3·5: The $0\overline{2}$ SM arc

3.6 Infinitely Many SM Spirals of Different Type

As $n+d$ increases, there are more and more choices for alternative upper right wedges. As previously stated, in the $(4, 5)$ case, both R_1^λ and R_2^λ satisfy Proposition 3.2.1. In the $(10, 7)$ case, $R_1^\lambda, R_4^\lambda, R_5^\lambda$, and R_6^λ all satisfy Proposition 3.2.1. In addition, for each spiral, there exist infinitely many preimages of that spiral in the parameter plane, as shown in figure 3·6. Note that a portion of the $0\overline{2}$ SM arc is depicted, as opposed to the $0\overline{2}$ SM spiral, because we do not know what it looks like. Also, the spirals are not drawn to be smooth, but that is purely an aesthetic choice - there is no requirement on the path a parameter λ takes through a Sierpinski hole.

The arbitrary choice of upper versus lower wedge together with $(n-1)$fold symmetry means that there are $2(n-1)$ as many spirals for each spiral we have shown to exist in the parameter plane. For $(4, 5)$, the SM hydra consists of the $0\overline{1}$ SM spiral and its infinitely many preimages the $0_k\overline{1}$ SM spirals, the $0\overline{2}$ SM spiral and its infinitely

many preimages the $0_k\overline{2}$ SM spirals, their reflections across the negative real axis, and their rotations in the other two sectors of the parameter plane.

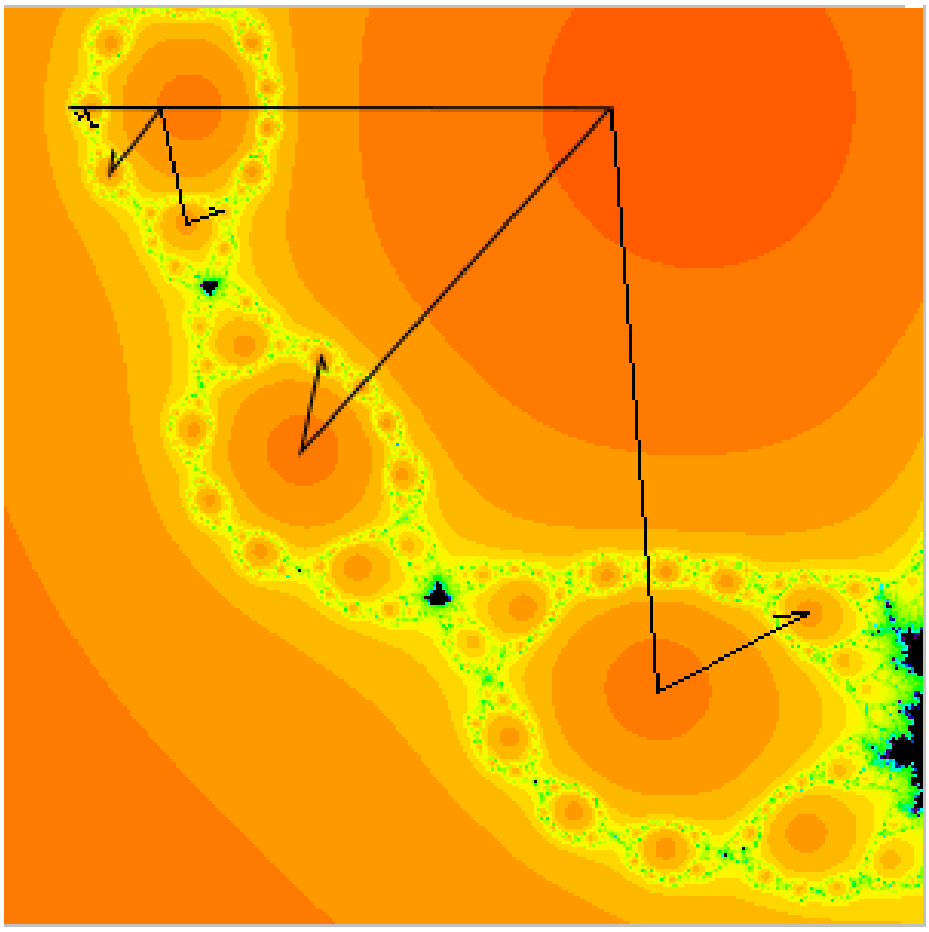

Figure 3·6: One sixth part of the SM hydra for $z^4 + \lambda/z^5$

List of Abbreviations for References

Amer. Math. Soc.	.....	American Mathematical Society
Ann. Sci. École Norm. Sup.	.....	Annales Scientifiques de l'École Normale Supérieure
Bull. Amer. Math. Soc.	.....	Bulletin of the American Mathematical Society
Contemp. Math.	.....	Contemporary Mathematics
Eur. Math. Soc.	.....	European Mathematical Society
Fund. Math.	.....	Fundamenta Mathematicae
Indag. Math.	.....	Indagationes Mathematicae
Indiana Univ. Math. J.	.....	Indiana University Mathematics Journal
Math. Sci. Res. Inst. Publ.	.....	Mathematical Sciences Research Institute Publications
N.S.	.....	New Series
Qual. Theory Dyn. Syst.	.....	Qualitative Theory of Dynamical Systems
Topology Proc.	.....	Topology Proceedings

References

Devaney, R. L. (2004). Cantor necklaces and structurally unstable Sierpinski curve Julia sets for rational maps. *Qual. Theory Dyn. Syst.*, 5(2):337–359.

Devaney, R. L. (2005). Structure of the McMullen domain in the parameter planes for rational maps. *Fund. Math.*, 185(3):267–285.

Devaney, R. L. (2006). Baby Mandelbrot sets adorned with halos in families of rational maps. In *Complex dynamics*, volume 396 of *Contemp. Math.*, pages 37–50. Amer. Math. Soc., Providence, RI.

Devaney, R. L. (2013). Singular perturbations of complex polynomials. *Bull. Amer. Math. Soc. (N.S.)*, 50(3):391–429.

Devaney, R. L. (2016). A Mandelpinski maze for rational maps of the form $z^n + \lambda/z^d$. *Indag. Math. (N.S.)*, 27(5):1042–1058.

Devaney, R. L. and Look, D. M. (2006). A criterion for Sierpinski curve Julia sets. *Topology Proc.*, 30(1):163–179. Spring Topology and Dynamical Systems Conference.

Devaney, R. L., Look, D. M., and Uminsky, D. (2005). The escape trichotomy for singularly perturbed rational maps. *Indiana Univ. Math. J.*, 54(6):1621–1634.

Devaney, R. L. and Russell, E. (2013). Connectivity of julia sets of singularly perturbed rational maps. pages 239–245.

Douady, A. and Hubbard, J. H. (1985). On the dynamics of polynomial-like mappings. *Ann. Sci. École Norm. Sup. (4)*, 18(2):287–343.

McMullen, C. (1988). Automorphisms of rational maps. In *Holomorphic functions and moduli, Vol. I (Berkeley, CA, 1986)*, volume 10 of *Math. Sci. Res. Inst. Publ.*, pages 31–60. Springer, New York.

Milnor, J. (2006). *Dynamics in one complex variable*, volume 160 of *Annals of Mathematics Studies*. Princeton University Press, Princeton, NJ, third edition.

Moreno Rocha, M. (2013). A combinatorial invariant for escape time Sierpiński rational maps. *Fund. Math.*, 222(2):99–130.

Roesch, P. (2006). On capture zones for the family $f_\lambda(z) = z^2 + \lambda/z^2$. In *Dynamics on the Riemann sphere*, pages 121–129. Eur. Math. Soc., Zürich.

CURRICULUM VITAE